AEMO
AUSTRALIAN ENERGY MARKET OPERATOR

Inverter-based resource controller design using frequency scanning techniques

November 2025

A report on the proof of concept exploring the application of the frequency scan methodology in inverter-based resource controller design

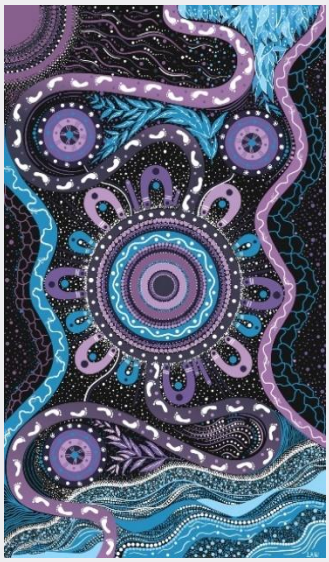

We acknowledge the Traditional Custodians of the land, seas and waters across Australia. We honour the wisdom of Aboriginal and Torres Strait Islander Elders past and present and embrace future generations.

We acknowledge that, wherever we work, we do so on Aboriginal and Torres Strait Islander lands. We pay respect to the world's oldest continuing culture and First Nations peoples' deep and continuing connection to Country; and hope that our work can benefit both people and Country.

'Journey of unity: AEMO's Reconciliation Path' by Lani Balzan

AEMO Group is proud to have launched its first Reconciliation Action Plan in May 2024. 'Journey of unity: AEMO's Reconciliation Path' was created by Wiradjuri artist Lani Balzan to visually narrate our ongoing journey towards reconciliation - a collaborative endeavour that honours First Nations cultures, fosters mutual understanding, and paves the way for a brighter, more inclusive future.

Important notice

Purpose

AEMO has prepared this document to provide information about a proof of concept conducted by AEMO exploring frequency scanning techniques used for controller design of inverter-based resources, as at the date of publication.

Disclaimer

The information in this document is provided for explanatory purposes and may be subsequently updated or amended. This document does not constitute legal, business, engineering or technical advice, and should not be relied on as a substitute for obtaining detailed advice about the National Electricity Law, the National Electricity Rules, or any other applicable laws, procedures or policies or the capability or performance of relevant equipment.

The National Electricity Law and the National Electricity Rules prevail over this document to the extent of any inconsistency.

AEMO has made reasonable efforts to ensure the quality of the information in this document but cannot guarantee its accuracy or completeness. Anyone proposing to use the information in this publication should independently verify its accuracy, completeness and suitability for purpose, and obtain independent and specific advice from appropriate experts.

Accordingly, to the maximum extent permitted by law, AEMO and its officers, employees and consultants involved in the preparation of this document:

- make no representation or warranty, express or implied, as to the currency, accuracy, reliability or completeness of the information in this document; and
- are not liable (whether by reason of negligence or otherwise) for any statements or representations in this document, or any omissions from it, or for any use or reliance on the information in it.

Copyright

Contents

Tables

Figures

Abbreviations and Definitions

Abbreviation	Definitions
AEMO	Australian Energy Market Operator
ACC	Alternating Current Controller
DFT	Discrete Fourier Transform
EMT	Electromagnetic transient
FRT	Fault ride through
GFL	Grid-following
GFM	Grid-forming
GPS	Generator and integrated resources provider performance standards
IBR	Inverter-based resources
LPF	Low-pass filter
ms	Milliseconds
MVA	Megavolt amperes
MVAR	Megavolt amperes reactive
MW	Megawatts
MPPT	Maximum Power Point Tracking
NEM	National Electricity Market
NER	National Electricity Rules
NSP	Network service provider
OEM	Original equipment manufacturer
PI	Proportional - integral
PLL	Phase-locked loop
PoC	Proof of Concept
PPC	Power plant controller
PCC	Point of common coupling
PSCAD™	Power Systems Computer Aided Design
PSS®E	Power System Simulator for Engineering
pu	Per-unit
RMS	Root mean square
SCR	Short circuit ratio
SG	Synchronous generator
SMIB	Single machine infinite bus
TF	Transfer function
VSC	voltage source converter
X/R	Reactance/resistance ratio

Background

This background provides an overview of a power system phenomena referred to as grid-scale oscillations, why they occur in all power systems, how they are managed to avoid disruptions and the assistance that small signal analysis can provide in mitigating issues in the planning and connection phase of power system development, well ahead of real time operations. Readers who are familiar with grid-scale oscillations may skip this section.

Voltage and power oscillations are a naturally occurring phenomena in electric power systems all over the world. If not planned and managed for, and the oscillations do not subside following a disturbance (e.g. a fault or sudden loss of generation or load), they have the potential to disrupt power systems. Power systems are therefore designed to automatically subdue these oscillations, a process referred to as damping. If an oscillation is undamped, due to unusual operating conditions, poor design or faulty equipment, it will grow, with a likely result being protection systems activating, leading to disconnection of loads, generation or even large sections of the power system.

AEMO and other network operators across the world are planning for and have observed an increase in oscillation events, primarily associated with decreasing synchronous (fossil-fuelled) generation and increasing inverter-based resources (solar, wind and battery energy storage systems). These oscillations often manifest themselves under conditions where system strength is decreased, such as a transmission line outage or periods of high solar and low synchronous generation.

System strength

System strength is the ability of the power system to maintain and control the voltage waveform at any location during both steady-state operation and following a disturbance. This definition reflects AEMO's *Power System Requirements*[1] and underpins the system strength reforms introduced through the AEMC's 2021 Efficient Management of System Strength rule change[2].

The current system strength management framework consists of two complementary requirements, set out in NER S5.1a.9 and implemented through AEMO's *System Strength Requirements Methodology*[3]:

- minimum three-phase fault level (system security requirement), and
- stable voltage waveforms (efficient level to host forecast IBR).

Each requirement plays a distinct role: minimum fault levels ensure reliable protection operation and system security, while stable voltage waveforms support the secure operation and connection of IBRs. These requirements are assessed at designated system strength nodes and may be further refined as technology and understanding evolve.

While both are critical to the stable operation of the power system, any discussion of system strength in this report refers to the ability for the power system to maintain and control a stable voltage waveform.

Power systems with many synchronous generators have high inertia characteristics due to the kinetic energy stored in the rotating masses of the generator and turbine. This inertia helps provide a stable frequency but can also result in low frequency (less than 0.5 Hz) oscillations between different regions of the grid, also known as inter-area oscillations. The

[1] At: https://www.aemo.com.au/-/media/files/electricity/nem/security_and_reliability/power-system-requirements.pdf

[2] At: https://www.aemc.gov.au/sites/default/files/2021-10/ERC0300 - Final determination_for publication.pdf

[3] At: https://www.aemo.com.au/-/media/files/electricity/nem/security_and_reliability/system-strength-requirements/system-strength-requirements-methodology.pdf

damping of inter-area oscillations has been kept at acceptable levels through the coordinated tuning of power system stabilisers (PSS) on a relatively small number of large synchronous generators. However, retirement of synchronous generators equipped with PSS is expected to reduce the number of PSS devices available to contribute to damping.

To account for the intermittent nature of renewable energy, new inverter-based resource generation is being deployed at many times the capacity (approximately 4:1) of synchronous generators exiting the system. This volume of inverter-based resources presents further challenges in the form of sub-synchronous oscillations (5-40 Hz), typically related to control system interactions among these resources.

Engineers are required to finely tune the control systems of inverter-based resources, to reduce the likelihood of these oscillations. The challenge with many controlled processes including power systems, is that they are non-linear, meaning there is not a linear relationship between a change in input and the response of the system. However, if the input change size is very small, the response of a system at a specific operating point, can be assumed as linear (linearisation). The engineer can then use existing linear-system tools to design and set control systems to give a stable response at a specific operating point. This technique is called small-signal analysis.

Small-signal analysis allows engineers to develop strategies to maintain adequate damping of all power system oscillations, including those related to inertia and control system interactions. AEMO currently uses small-signal analysis to quantify the level of damping for an oscillation and, importantly, facilitate the design of control systems that can improve this damping, resulting in a more stable power system which is resilient to disturbances.

Executive summary

The capacity of the National Electricity Market (NEM) will need to increase significantly by 2050 (to roughly treble of its existing capacity) in order to supply sufficient energy to replace retiring fossil-fuelled generation capacity and meet increased demand as Australia decarbonises through electrification[4]. Growth in the NEM's energy generation and battery storage capacity is primarily in inverter-based resources (IBRs). Large volumes of IBRs may result in greater levels of sub-synchronous oscillations (SSOs) from interactions between IBRs. The control systems on these IBRs therefore need to be carefully managed and planned to mitigate the potential for SSOs and increased risks to power system security.

Currently SSOs are identified through electromagnetic transient (EMT) simulation, however, this analysis is time-consuming, computationally intensive and issues can be overlooked in the detailed and complex study results. An independent review into future requirements for power system analysis tools was conducted in 2024 to investigate potential improvements to the generator connections assessment process[5]. The review found SSOs could be mitigated by improving the tuning of IBR controllers early in the connections assessment process using small-signal analysis tools.

Using small-signal analysis to robustly and efficiently design IBR controllers is not a new concept. Small-signal and eigenvalue analysis using specialised models are utilised in the design of synchronous generator controllers. Frequency scanning, a small-signal analysis method, is attracting significant interest as it allows system dynamics observable in time domain EMT simulations to be analysed in the frequency domain, while utilising existing PSCAD™ EMT models.

Analysing system dynamics in the frequency domain using frequency scanning presents many potential operational and planning applications. These include assessing the stability and robustness of IBR control systems, informing the development of control system parameter settings and protection schemes, determining whether individual generating systems are participating in oscillation events and synthesising Resistor Inductor Capacitor (RLC) equivalent circuits of individual generating systems or sections of the power system.

Although numerous emerging applications of this method are being explored by AEMO, universities, system and network operators, this report is focused on the feasibility, benefits, and potential applications of frequency scanning within the connections process through a structured proof of concept (PoC).

Use of frequency scanning terminology

Frequency scanning is considered a general system identification technique to analyse the small-signal behaviour of an electrical system. Impedance and admittance scanning are considered methods within frequency scanning, with immittance scanning representing the combination of these methods. While they each have their own specific methodology in how they are calculated, for the purpose of this document the terms should be treated as interchangeable.

The primary goal of the PoC is to confirm that frequency scanning tools will enable project proponents to tune their IBR controllers in a manner that reduces the risk of stability problems, such as those caused by IBR control system interactions. This will enhance and streamline the connection process for assessing the ability for generators to securely operate in the

[4] At: https://aemo.com.au/-/media/files/major-publications/isp/2024/2024-integrated-system-plan-isp.pdf?la=en

[5] At: https://aemo.com.au/energy-systems/electricity/national-electricity-market-nem/participate-in-the-market/network-connections/power-system-analysis-tools

power system by introducing a methodical tuning process that reduces the risk of issues being uncovered in wide area PSCAD™ studies, during the full assessment (FA) process undertaken by the Network Service Provider (NSP), and due diligence process undertaken by AEMO.

The first three stages of the PoC, which focused on applying the method to simple scenarios, are complete and show significant merit in the proposed application of tuning IBR controllers. Testing in these PoC stages confirms improved controller tuning can be achieved, providing confidence the method can assist in identifying SSOs early in the connection assessment process.

The proof of concept is structured in stages with increasing complexity, starting with simple tests with known outcomes and progressing to demonstrating the method on active generator connection projects. The proof of concept is intended to validate the frequency scan method and identify practical issues from applying it. The stages are:

- **Stage 1:** Validation of the frequency scan stability analysis method using a known (white box) and encrypted (black box) IBR model.
- **Stage 2:** Frequency scan design of controller settings for stability in single machine infinite bus configuration.
- **Stage 3:** IBR controller design in wide area model.
- **Stage 4:** Generator connection project trial involving a minimum of four active projects to provide confidence in the approach.

Stages 1, 2 and 3 are complete. Stage 4 commenced late-Q2 2025 and is expected to be completed in 2026. Stage 4 may be extended to include additional projects or applications, subject to interest from Proponents and Network Service Providers.

Although the current PoC is focussed only on the utility of controller design to mitigate against SSOs, the technique has further applications in power system analysis. An example of this is demonstrated in a joint analysis by AEMO and the National Renewable Energy Laboratory (NREL)[6], where the technique was successfully used to identify the root-cause of oscillations and develop remediation measures.

Proof of concept objectives

The PoC is intended to demonstrate the practical application of the frequency scan method by investigating:

- The functionality of the frequency scanning tool applied in a PSCAD™ model to generate frequency scans of the IBR and power system.
- The frequency range that should be used for controller tuning, and how frequencies are simulated (as a composite signal of many frequencies or one frequency at a time).
- The size of the perturbation used to identify the plant and system frequency response from which transfer functions (TFs) can be estimated.
- The robustness of the method to account for cross coupling between different sets of axes (for example, d-q axes or positive-negative sequence impedances).

On successful completion of the PoC, the following outcomes are expected:

- Confirmation that the accuracy of the TF obtained using frequency scans is sufficient for controller tuning.
- Any limitations in frequency bands for which the method provides valid results.

[6] At: https://aemo.com.au/-/media/files/initiatives/engineering-framework/2025/analysis-of-sub-synchronous-oscillation-in-west-murray-zone-power-system-in-australia---external.pdf?la=en

- Strengths, weaknesses and assumptions of different frequency scan tools and approaches.
- Benchmarking of frequency scan methods against existing tools and quantifying any differences.
- Assessment of the time taken to perform scans on wide area EMT models in PSCAD™.

Stages 1 - 3 provide initial findings on these points for the simple models analysed.

Stage 1 – Validation of single models

Stage 1 of the PoC is split into two sub-stages and aims to validate the frequency scan analysis method for two scenarios using a simple single machine infinite bus (SMIB) model.

Stage 1.1 – White box validation

The white box model was developed from literature[7], and is representative of IBRs in the NEM. The advantage of using a white box model is that it is possible to calculate the TF analytically, giving a reference that can be used to validate the frequency scan method. For this analysis, a d-q set of axes is selected because the model description is in the same set of axes.

The white-box validation highlights complexities with the physics of the IBR plant, such as cross coupling between the d and q-axis or between positive and negative sequence reference frames. This leads to complexities in visualising and interpreting the results. However, the frequency scan method is valuable for evaluating the stability of the generating system under assessment. Comparing the theoretical and measured results, presented as a series of Bode plots, shows:

- Close alignment is achieved between the theoretical results and the individual measurements for each frequency.
- A slight deviation between theoretical and measured results at low frequencies, below 3 Hz.

Similar accuracy is obtained when model parameters were varied, indicating a robustness for the scanning process and providing confidence in the technique. The deviations between theoretical and measured results at low frequencies can be improved by careful adjustment of frequency scan parameters such as perturbation magnitude, use of single or composite signals, and simulation step size.

Stage 1.2 – Black- box IBR model validation

Stage 1.2 is an extension of the white box model validation, except it is no longer possible to calculate the TF analytically to use as a reference. For the case of the black box model validation, the model is analysed in the frequency domain and validated against results in the time domain using EMT simulations. A model representing an operational solar plant located in a weak location of the NEM, which has a history of SSOs, is used as the black box IBR model.

The frequency scans are derived by measuring responses in EMT simulations and analysing results with frequency scan tools. This allows the parameters of the model to be adjusted to obtain a marginally stable response. These same cases are then tested in EMT simulations to confirm the same characteristics are observed in both the time and frequency domains.

[7] Zhou W, Mohammed N, Bahrani B. “Comprehensive modelling, analysis, and comparison of state-space and admittance models of PLL-based grid-following inverters considering different outer control modes” IEEE Access, 2022, 10: 30109-30146.

The frequency scan predictions for marginally stable and marginally unstable translate well in the time domain, which exhibit the expected performance. The points of instability located using the frequency scan method and EMT studies agree closely, reflecting the accuracy of the method.

The results confirm that the frequency scanning method can accurately identify the stability boundary and resonance frequency of the black box IBR under various short-circuit ratio (SCR) conditions.

Stage 2 – Design of controller settings for stability

In Stage 2, the frequency scan method is used to adjust the controller parameters to improve the stability of the black box model used in Stage 1.2. This is an important step as the primary objective of the PoC is to demonstrate the tuning of IBRs to improve stability.

Starting with a known unstable condition, the phase-locked loop (PLL) parameters are adjusted to increase the damping factor and achieve adequate gain and phase margins. This is an iterative process but relatively quick as it only requires use of a simple SMIB model in the frequency domain.

This analysis highlights the ability of the frequency scan method to examine the stability of a practical IBR model when connected to the power system and to adjust parameters, in this case the PLL damping, to achieve a satisfactory level of stability. Conventional control system methods, using Nyquist and Bode plots, are used to provide a clear visual representation of the design process and the transition from unstable to stable behaviour.

Stage 2 demonstrated the concept of taking adverse operating conditions and successfully achieving stable performance in relatively short time, when comparing to a traditional time domain approach. In practice, generating system controller settings need to be validated to ensure they are achievable with the equipment and agreed generator and integrated resources provider performance standards.

Stage 3 – Controller design in wide area network

Stage 3 examines how a proponent can use the frequency scan method to connect a new IBR to the grid, addressing complex dynamics of nearby IBR systems and mitigating issues found in wide area EMT studies. The flow chart in Figure 1 and following description explains the methodology used in this stage to demonstrate how the frequency scan method can assist in the IBR controller tuning for wide area studies.

Figure 1 IBR controller design in wide area network methodology

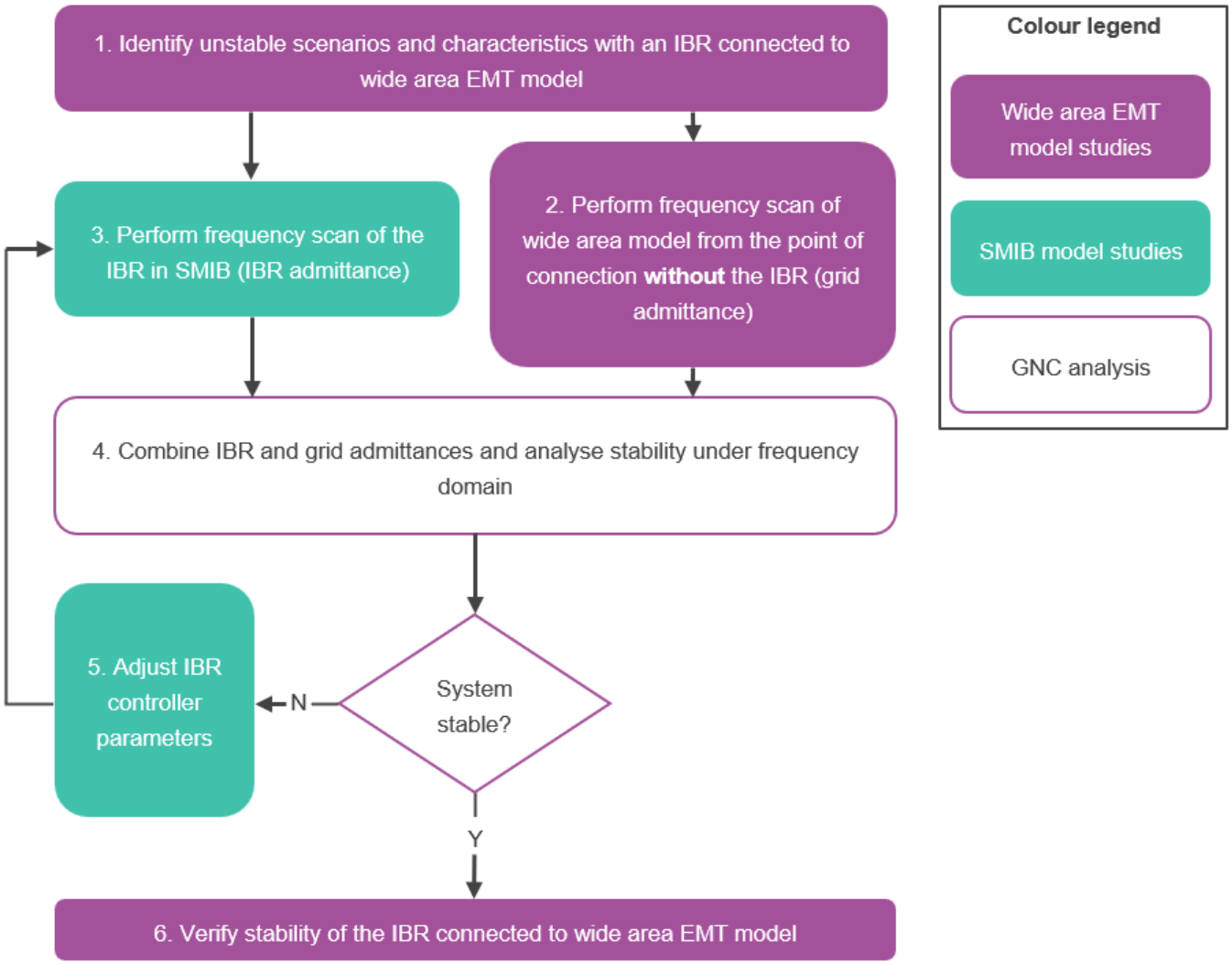

1. A baseline frequency scan of the IBR under assessment while connected to the wide area EMT model is performed to capture unstable characteristics.
2. The IBR is then disconnected, and a frequency scan is performed looking into the wide area EMT model from the point of connection of the IBR, providing a whole of grid admittance.
3. The IBR admittance is obtained through a frequency scan in a SMIB configuration
4. The IBR admittance is combined with the whole of grid admittance to assess the stability using Generalized Nyquist Criterion (GNC), allowing the gain and phase margins to be easily understood for the IBR.
5. If the gain and phase margins are not adequate for stability, the IBR model control parameters are modified, with a new frequency scan generated in the SMIB configuration and assessed for stability as before. This process is repeated until the GNC plot of the combined IBR and grid admittance confirms adequate gain and phase margins, indicating a stable controller design.

6. The new tuned IBR model is integrated back into the wide area EMT model and validation of the tuned IBR was performed in time domain simulations. The close alignment of the outcomes in the frequency domain and time domain confirms that frequency scanning can be used to accurately tune IBR controllers to achieve system stability in complex networks.

It is important to note that the controller tuning process (steps 3 to 5) does not require repeated wide area frequency scans, only a single wide area scan is required for each set of network operating conditions. The IBR needs to be rescanned for each new set of control parameters, however, this is a relatively quick process as the simulations are performed in a simple SMIB model.

The frequency scan method provides distinct advantages over time-domain tuning of IBRs using the wide area EMT model. This is primarily since much of the iterative tuning process can be conducted through SMIB simulations, which typically require only minutes per iteration, in contrast to the several hours needed per iteration with the wide area model. Additionally, the frequency scan method offers clear indications of stability margins, enabling engineers to achieve the desired level of resilience and reduce the number of required iterations.

Key outcomes and further work

Stage 1 demonstrated that for IBRs connected in a simple SMIB model, the frequency scan method can:

- Replicate the method described in academic literature to produce a TF that accurately aligns with a theoretical TF derived from the white box model. Deviation from the theoretical TF was observed at low frequencies, however, this deviation can be minimised by prudent selection of frequency scan input parameters.
- Produce a TF of a black box model that is sufficiently accurate to determine the point at which instability occurs when a single variable (such as SCR) is changed. For the same conditions, the time domain simulations in EMT were found to closely replicate the stability inflexion points observed using the frequency scan method.

Stage 2 examined how controller parameters could be tuned to improve the stability of the IBR. The results demonstrate the ability to:

- Provide a visual representation of the impact parameter changes have on control system stability.
- Analyse stability over a range of frequencies in a single study.
- Utilise conventional stability measures such as gain and phase margins to guide the tuning process.

Stage 3 demonstrated that frequency scan methods can be effectively applied to wide area network models. The results demonstrated:

- Whole of grid admittance and IBR admittance in SMIB scenarios can be independently produced and reconstructed at the point of connection in a SMIB model to tune IBR control parameters through GNC plots.
- The approach significantly reduces the need for repeated time domain simulations in wide area EMT models, showcasing its potential for a faster and transparent controller tuning process in large complex system conditions.
- Proponents are able to consider the dynamics in the wide area model when setting IBR controllers, without requiring AEMO to provide access to the wide area model or confidential EMT models. Considering wide area dynamics allows for improved stability across various operating conditions compared to approaches that depend

on SMIB studies with equivalent impedances. This will reduce the risk of substantial rework if stability issues are discovered by AEMO or the NSP during their wide area assessments in EMT.

During Stages 1 to 3, the following limitations were observed:

- The frequency scan method has settings related to the amplitude of the voltage or current perturbation used to measure the TF. Initial observations indicate this amplitude varies depending on the frequency and explains the observed deviations in theoretical and measured results at low frequencies. Further work is in progress investigating the optimal amplitude for low frequency perturbations.
- The cross-coupling effect makes visualisation of the data challenging. The wider industry is anticipated to experience an adaptation period in order to effectively utilise these tools and accurately interpret their outputs.

1 Introduction

As the penetration of inverter-based resources (IBR) such as solar and wind continues to grow within modern power systems, maintaining the stability and reliability of the electricity grid has become a complex and pressing challenge. Synchronous generators are steadily being replaced or supplemented by IBRs governed by advanced control systems with significantly different capabilities to traditional synchronous generation control schemes. This shift introduces new dynamic behaviours and potential interactions that may compromise system stability, particularly under scenarios with high penetration of IBRs.

To address these challenges, robust methodologies are essential for analysing and designing IBR controllers that can maintain stable operation across a range of network scenarios and operating conditions. One promising approach is the use of frequency scan techniques to evaluate controller performance and the potential for adverse interactions. By methodically injecting perturbation signals and measuring system responses, frequency scanning enables detailed insights into the dynamic characteristics and stability margins of both IBRs and their performance within the wider grid.

This document presents a comprehensive PoC developed by AEMO, structured in four stages, to assess how frequency scan methods can support engineers in tuning IBR controllers for robust operation. This PoC investigates the role of stability analysis and controller design, explores their application in IBR integration into wide area networks, and lays the groundwork for future pilot projects. Through this initiative, the goal is to increase confidence in connection study submissions, streamline engineering assessments, and ultimately enhance the stability and reliability of Australia's evolving power system.

2 Frequency scan methodology

The frequency scan method is a process used to measure and analyse the response of a system across a range of frequencies to identify resonances and dynamic characteristics. Frequency scanning is used to obtain response measurements of IBR models at multiple frequencies across numerous operating conditions. The method involves injecting a voltage and measuring a resulting current, the ratio of the current and voltage response is effectively an impedance or admittance. EMT studies are utilised for injecting and measuring responses, as EMT models currently provide the highest level of detail in the NEM.

The key elements of the EMT-based measurement method are:

- Frequency scan module: Injects the perturbation signal and measures the responses.
- Measurement approach: The signal is injected in both d-axis and q-axis to obtain all four elements of the 2x2 impedance matrix[8].
- Frequency scanning tool: An inhouse developed frequency scanning tool was used in the proof of concept.
- Perturbation frequencies: Selects frequencies for the perturbations and the magnitude of injected signals.
- Operating conditions: The admittance frequency responses of the IBR may vary with different operation conditions (i.e. IBR operating points, control parameters and grid conditions).

2.1 Frequency scan module

The EMT-based frequency scanning module shown in Figure 2, injects voltage perturbation signals at various frequencies into both the grid and the IBR, capturing the current response to assess admittance. To accurately determine the frequency scan in the dq frame[9] along with the cross coupling between these axes, perturbations must be applied in both axes.

Figure 2 Configuration of the EMT-based frequency scan setup in a SMIB system

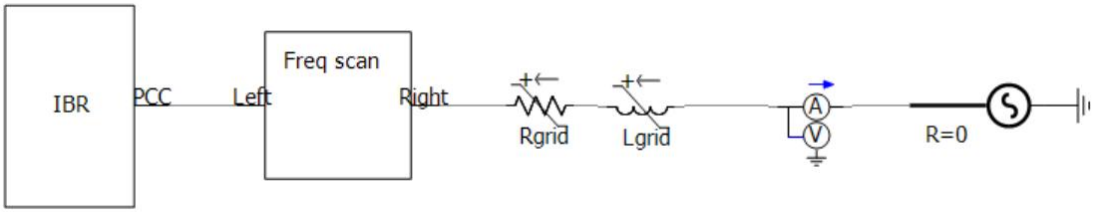

The perturbations are applied from a voltage source (v_{pert}) in the d-axis and q-axis, respectively, as shown in Figure 3. In order to inject a dq-axis perturbation in PSCAD™, the following approach is adopted:

- A three phase balanced voltage source is configured.

[8]The impedance in dq axis can be transferred to sequence-domain to analyse stability features in the positive- and negative-sequence domain

[9] The dq frame is a widely used technique used for analysing three phase systems that transforms the ac system frame (abc) into a rotating reference frame (Dq0).

- The total perturbation voltage amplitude is normally set to between 5% and 10% of the Point of Common Coupling (PCC) voltage magnitude.
- The phase shift relative to the inverter terminal voltage is set to zero in the d-axis and 90 degrees in the q-axis.
- The q-axis and d-axis voltage perturbation is designed to be zero in d-axis and q-axis perturbations, respectively.
- The IBR is set to an initial operating point by adjusting the current reference.
- The currents that result from the perturbations are processed into d- and q-axis components to give admittance frequency responses in both the injected axis and the cross coupled axis.

Figure 3 Equivalent circuit of the frequency scan module for IBR

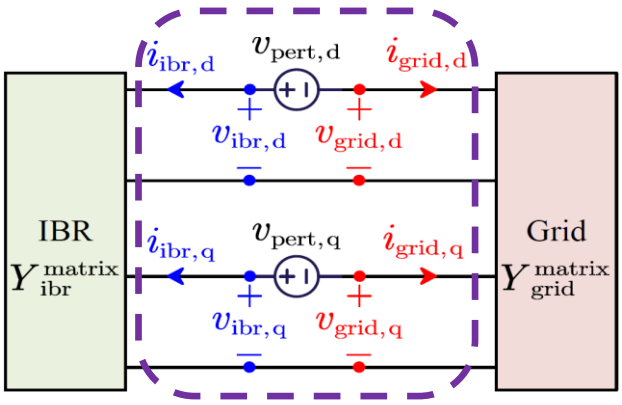

2.2 Measurement approach

The approach to identifying the IBR impedance is to inject separately in the direct- and then the quadrature-axis. For each injection, the responses in both axes are measured as presented in Figure 4. The responses to the injection are measured to obtain:

For the direct-axis injection:

- Y_{dd} – the current response in the d-axis for a perturbation in V_d
- Y_{qd} – the current response in the q-axis for a perturbation in V_d

For the quadrature-axis injection:

- Y_{dq} – the current response in the d-axis for a perturbation in V_q
- Y_{qq} – the current response in the q-axis for a perturbation in V_q

Figure 4 Equivalent circuit of the voltage perturbation in d and q axes

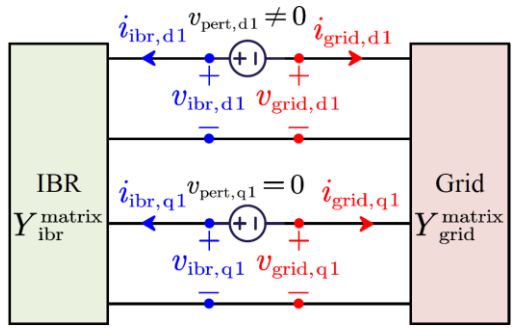

(a) D-axis voltage perturbation using $v_{pert,d1} \neq 0$ V and $v_{pert,q1}=0$

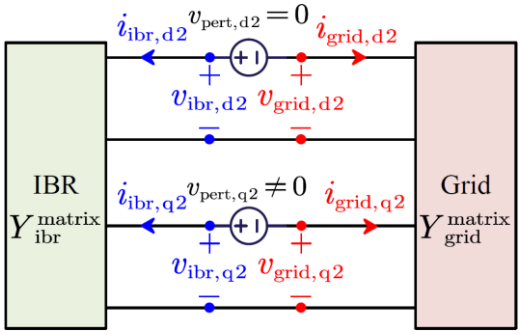

(b) Q-axis voltage perturbation using $v_{pert,d2}=0$ and $v_{pert,q2} \neq 0$

In the first-round measurement, the d-axis voltage perturbation is injected, as shown in Figure 4(a)[10]. According to Ohm's law, the following equation can be established:

$$\text{IBR side: } \begin{bmatrix} \mathcal{F}(i_{\mathrm{ibr,d1}}) \\ \mathcal{F}(i_{\mathrm{ibr,q1}}) \end{bmatrix} = \begin{bmatrix} Y_{\mathrm{ibr,dd}} & Y_{\mathrm{ibr,dq}} \\ Y_{\mathrm{ibr,qd}} & Y_{\mathrm{ibr,qq}} \end{bmatrix} \begin{bmatrix} \mathcal{F}(v_{\mathrm{ibr,d1}} \neq 0) \\ \mathcal{F}(v_{\mathrm{ibr,q1}} = 0) \end{bmatrix}$$
$$\text{Grid side: } \begin{bmatrix} \mathcal{F}(i_{\mathrm{grid,d1}}) \\ \mathcal{F}(i_{\mathrm{grid,q1}}) \end{bmatrix} = \begin{bmatrix} Y_{\mathrm{grid,dd}} & Y_{\mathrm{grid,dq}} \\ Y_{\mathrm{grid,qd}} & Y_{\mathrm{grid,qq}} \end{bmatrix} \begin{bmatrix} \mathcal{F}(v_{\mathrm{grid,d1}} \neq 0) \\ \mathcal{F}(v_{\mathrm{grid,q1}} = 0) \end{bmatrix}$$

Where *F* denotes the Discrete Fourier Transform (DFT) operator, solving the above equation leads to the dd- and qd-axis admittance components as:

$$\text{IBR side: } Y_{\mathrm{ibr,dd}} = \frac{\mathcal{F}(i_{\mathrm{ibr,d1}})}{\mathcal{F}(v_{\mathrm{ibr,d1}})}, \quad Y_{\mathrm{ibr,qd}} = \frac{\mathcal{F}(i_{\mathrm{ibr,q1}})}{\mathcal{F}(v_{\mathrm{ibr,d1}})}$$
$$\text{Grid side: } Y_{\mathrm{grid,dd}} = \frac{\mathcal{F}(i_{\mathrm{grid,d1}})}{\mathcal{F}(v_{\mathrm{grid,d1}})}, \quad Y_{\mathrm{grid,qd}} = \frac{\mathcal{F}(i_{\mathrm{grid,q1}})}{\mathcal{F}(v_{\mathrm{grid,d1}})}$$

In the second-round measurement, the q-axis voltage perturbation is injected, as shown in Figure 4(b). According to Ohm's law, the following equation can be established:

[10] Shen Z, Jaksic M, Mattavelli P, et al. Design and implementation of three-phase AC impedance measurement unit (IMU) with series and shunt injection[C]//2013 Twenty-Eighth Annual IEEE Applied Power Electronics Conference and Exposition (APEC). IEEE, 2013: 2674-2681.

$$\text{IBR side: } \begin{bmatrix} \mathcal{F}(i_{\text{ibr,d2}}) \\ \mathcal{F}(i_{\text{ibr,q2}}) \end{bmatrix} = \begin{bmatrix} Y_{\text{ibr,dd}} & Y_{\text{ibr,dq}} \\ Y_{\text{ibr,qd}} & Y_{\text{ibr,qq}} \end{bmatrix} \begin{bmatrix} \mathcal{F}(v_{\text{ibr,d2}} = 0) \\ \mathcal{F}(v_{\text{ibr,q2}} \neq 0) \end{bmatrix}$$
$$\text{Grid side: } \begin{bmatrix} \mathcal{F}(i_{\text{grid,d2}}) \\ \mathcal{F}(i_{\text{grid,q2}}) \end{bmatrix} = \begin{bmatrix} Y_{\text{grid,dd}} & Y_{\text{grid,dq}} \\ Y_{\text{grid,qd}} & Y_{\text{grid,qq}} \end{bmatrix} \begin{bmatrix} \mathcal{F}(v_{\text{grid,d2}} = 0) \\ \mathcal{F}(v_{\text{grid,q2}} \neq 0) \end{bmatrix}$$

Solving the above equation leads to the dq- and qq-axis admittance components as:

$$\text{IBR side: } Y_{\text{ibr,dq}} = \frac{\mathcal{F}(i_{\text{ibr,d2}})}{\mathcal{F}(v_{\text{ibr,q2}})}, \quad Y_{\text{ibr,qq}} = \frac{\mathcal{F}(i_{\text{ibr,q2}})}{\mathcal{F}(v_{\text{ibr,q2}})}$$
$$\text{Grid side: } Y_{\text{grid,dq}} = \frac{\mathcal{F}(i_{\text{grid,d2}})}{\mathcal{F}(v_{\text{grid,q2}})}, \quad Y_{\text{grid,qq}} = \frac{\mathcal{F}(i_{\text{grid,q2}})}{\mathcal{F}(v_{\text{grid,q2}})}$$

After two rounds of admittance measurements, the four admittance elements of the dq-domain admittance matrices of both the IBR and grid can be obtained by the frequency scanning module.

2.3 Frequency scanning tool

The Frequency-domain Admittance-based Stability Tool (FAST) is a graphical interface developed by AEMO[11] to support the frequency scan stability analysis of inverter-based resources (IBRs) in power systems. Built in Python and integrated with PSCAD™, FAST automates the process of injecting small perturbations across a range of frequencies, measuring system immittance, and visualizing the results using tools such as Bode plots and Nyquist diagrams.

FAST was developed specifically to assist with the investigation and validation of the frequency scan proof of concept. Its purpose is to provide a practical and efficient platform for testing how frequency scan techniques can be applied to real-world power system analysis.

FAST was developed in late 2024, since then several commercial and open-source frequency scanning tools have been released. AEMO has benchmarked FAST against these tools with positive results, as described further in section A1.5.

2.4 Perturbation frequencies

To ensure meaningful and accurate impedance measurements across a wide frequency range, the perturbation signal should be carefully designed by considering both spectral coverage and system response characteristics. The selection of perturbation frequencies typically follows a logarithmic distribution, effectively capturing both low- and high-frequency dynamics. The perturbation amplitude must be sufficiently small to maintain linear system behaviour while still enabling a measurable response above the numerical noise floor. Moreover, the duration of the perturbation should be chosen to allow steady-state convergence, particularly for the lowest frequency components, which require longer simulation time intervals to complete multiple cycles.

The frequency scan method supports single frequency injections or a composite of multiple frequencies. In this study, a method of simultaneous injection of multiple frequencies (multi-tone) is employed to enhance computational efficiency, while the DFT is utilised to isolate individual frequency-admittance points.

[11] This tool was developed in-house utilising open-source elements due to delays in accessing commercial tools.

2.5 Operating conditions

Frequency scan analysis should consider different operating points of the IBR, control parameters and grid conditions. These conditions can include:

- Different operating points: irradiance, active power, reactive power, DC-link voltage, voltage at the point of connection, active current and reactive current setpoint.
- Control parameters: Maximum Power Point Tracking (MPPT), active power controller, reactive power controller, DC-link voltage controller, PCC voltage controller, active current controller and reactive current controller, PLL controller.
- Grid condition: different SCRs and X/R ratios.

3 Stage 1: Validation of frequency scan stability analysis

Stage 1 of the PoC focused on validating the frequency scan method using both white box (system with known transfer function) and black box (hidden internal structure) models of IBRs. This validation provides initial confirmation that frequency scan methods can accurately and reliably capture critical small-signal characteristics, as anticipated by theoretical white box models or by EMT simulations for black box models. This provides a critical foundation to guarantee the methodology's relevance in both theoretical and practical contexts, thereby supporting effective controller tuning in future applications.

3.1 White box IBR model

The white box IBR is connected to the grid through an impedance that consists of both grid resistance and grid reactance in a simple SMIB configuration, as described previously in Figure 2 above. A frequency scan block is placed between the IBR model and grid impedance, minimally affecting system dynamics. A meter on the right side of the grid impedance measures the grid voltage (V_{grid}) and current (I_{grid}). The grid voltage and frequency are defined as 1 pu and 50 Hz respectively.

There are five steps in this process:

1. Obtain the theoretical frequency responses based on transfer functions, represented by Bode plots.
2. Develop a PSCAD™ model of the system in a SMIB configuration.
3. Use a frequency scan block to identify the impedance frequency responses of the system.
4. Compare the theoretical and derived impedance frequency responses.
5. Discuss differences and understand the causes of any discrepancies.

A detailed description of the white box model used is provided in Appendix A1.1.

3.1.1 Approach

The frequency scan parameters are as follows:

- Scanned frequency range: 80 frequency points logarithmically distributed between 1 Hz and 2500 Hz (see Appendix A1.4).
- Perturbation magnitude: 0.125% of the steady-state PCC voltage per frequency component, resulting in a peak of 10% when all components are co-phasal.
- Simulation step time: 50 microseconds (µs).
- Initial phase shift: 0 degrees for all frequency components.
- Perturbation duration: 20 s, allowing the lowest frequency to complete enough cycles to reach steady state.

For this test, the IBR is initially set to have an active current reference of 0.5 pu at an angle of zero degrees relative to the terminal voltage (d-axis). The PLL parameters are initially set to Kp_{PLL}=22 and Ki_{PLL}=242. For subsequent measurements, the active current reference is changed to explore the range of admittance frequency responses. The grid SCR is set to 20 to produce a sufficient stability margin.

Similarly, for further validation purposes, the active current reference is maintained at 1 pu, and the PLL parameters are adjusted from their initial parameters.

3.1.2 Analysis and validation

The input voltage signal, composed of the 80 frequency points, and observed current responses are shown in Figure 5. The IBR is initially set to have an active current reference of 0.5 pu at an angle of zero degrees relative to the terminal voltage (d-axis). The d- and q-axis voltage perturbations are injected from 5 s to 25 s and from 25 s to 45 s, respectively. Note there is a spike in the injected signals that arises as the phase angles of the individual frequencies are set to zero, giving a summated value initially equal to the arithmetic sum of the individual components. In cases where there is a concern that these spikes may cause non-linear behaviours, the input signal can be modified to restrict the peak amplitude.

Figure 5 also shows the measured responses of IBR current in dq frame (Id_meas and Iq_meas). These responses demonstrate that cross coupling occurs, as injecting a signal in the d-axis generates a response in the q-axis and vice versa.

Figure 5 EMT measurement during the two rounds of voltage perturbation

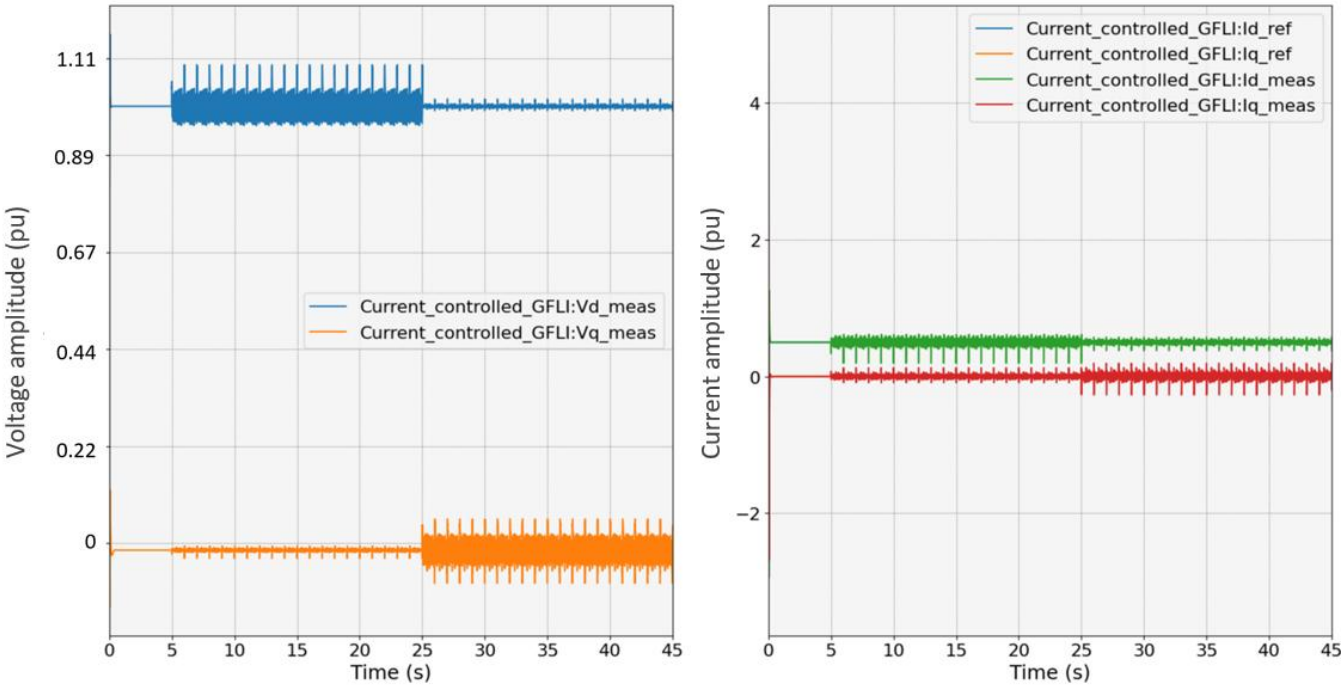

Figure 6 presents the Bode diagrams of the four admittance components calculated from the measured responses. An important observation here is that the off-diagonal terms, Y_{dq} and Y_{qd}, have a material magnitude in the 10-100 Hz band, relative to the diagonal elements. Outside of this 10-100 Hz range, the magnitude of the off-diagonal terms decreases rapidly. This implies that for frequencies above 100 Hz or frequencies below 10 Hz, the off-diagonal terms become less

significant, and the admittance matrix could potentially be approximated by the diagonal terms only. The following observations apply:

- The off-diagonal elements are less significant below 10 Hz as no reactive power is injected in this case study (reactive power injection can increase the cross coupling between the d and q axes). In cases where there is reactive injection, the cross coupling at low frequency may be more pronounced. In general, it is better not to approximate the impedance matrix with diagonal-only terms for low frequency analysis.
- The off-diagonal elements are less significant above 100 Hz as the IBR's small-signal dynamics in this frequency range is mainly determined by the fast current control loop and digital time delay which can be depicted by diagonal admittance matrices with negligible off-diagonal admittance elements.

The initial frequency scan implemented a fixed operating point and PLL settings. Stage 2 explores varying these settings to assess the impact of the results.

Figure 6 Bode plots of measured admittance at IBR terminal

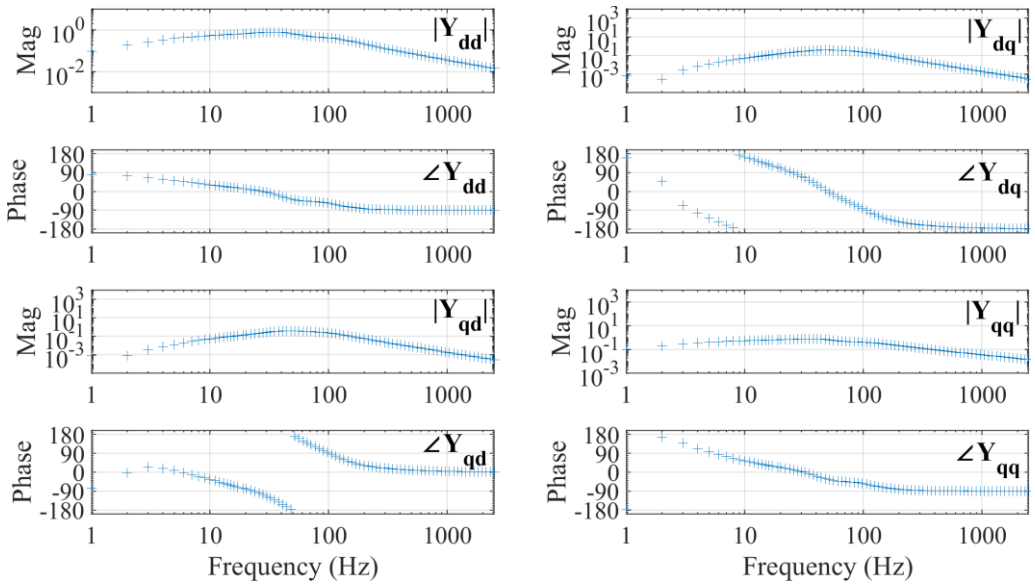

To validate the accuracy of the frequency scanning results, Bode plots of the theoretical model are overlayed on the measured admittance frequency response for different active power levels. Figure 7 shows the comparison as the active current reference changes from 0.3 to 0.9 pu. In all cases, the reactive current is kept at 0 pu, with the PLL parameters K_{pPLL} = 22, K_{iPLL} = 242. It can be seen from both the figures that the theoretical and measured Bode plots exhibit very good agreement. However, a minor discrepancy typically less than 10% is observed below 3 Hz for the dq- and qd-axis admittance components. The cause of the low frequency discrepancies is discussed in Section 3.1.3.

Figure 7 Measured and theoretical admittance at IBR terminal with different operating points

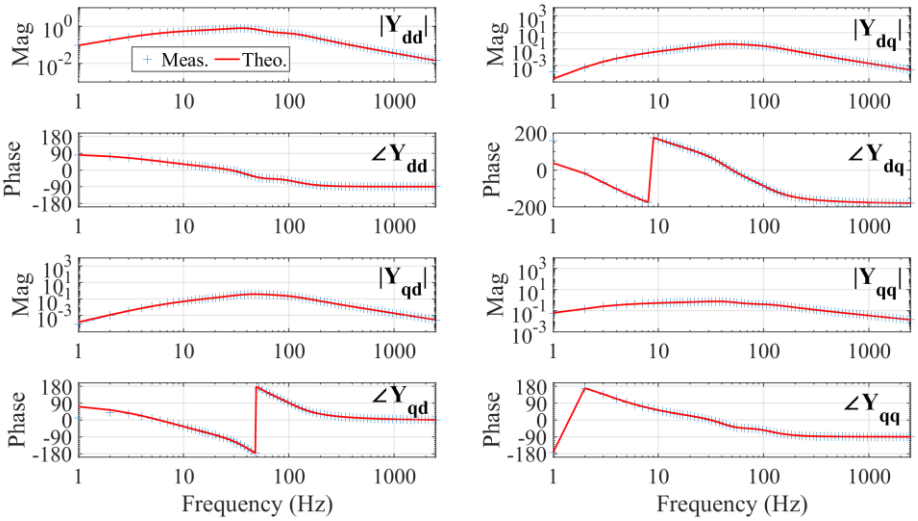

(a) Active current of IBR is 0.3 pu

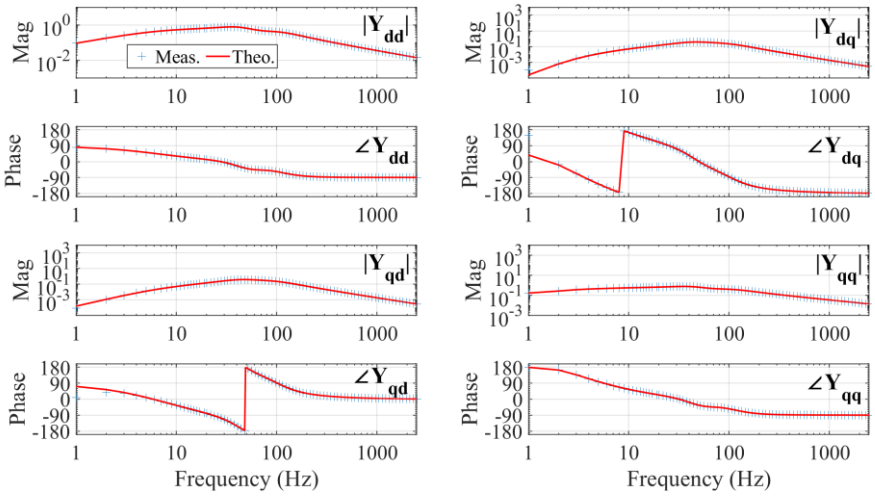

(b) Active current of IBR is 0.9 pu

Figure 8 further demonstrates the accuracy of the frequency scanning results. The Bode plots of these results show the theoretical and measured admittance frequency response as the PLL parameters $(K_{\mathrm{pPLL}}, K_{\mathrm{iPLL}})$ are changed from (10, 50) to (60, 1800), while the active current reference is 1.0 pu and the reactive current is 0 pu. Again, it is observed that the theoretical and measured Bode plots exhibit very good agreement; however, a minor discrepancy is noted below 3 Hz regarding the dq- and qd-axis admittance components.

Figure 8 Bode plots of measured and theoretical admittance at IBR terminal with different control parameters

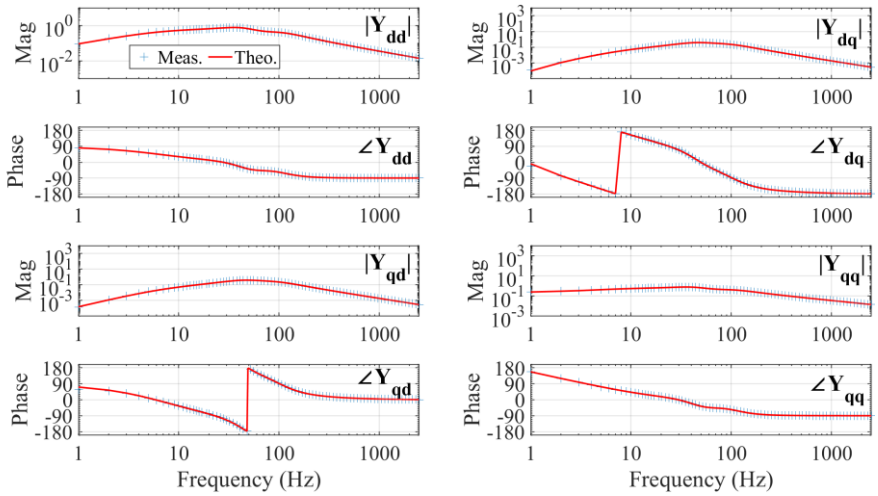

(a) PLL parameters $K_{\mathrm{pPLL}} = 10, K_{\mathrm{iPLL}} = 50$

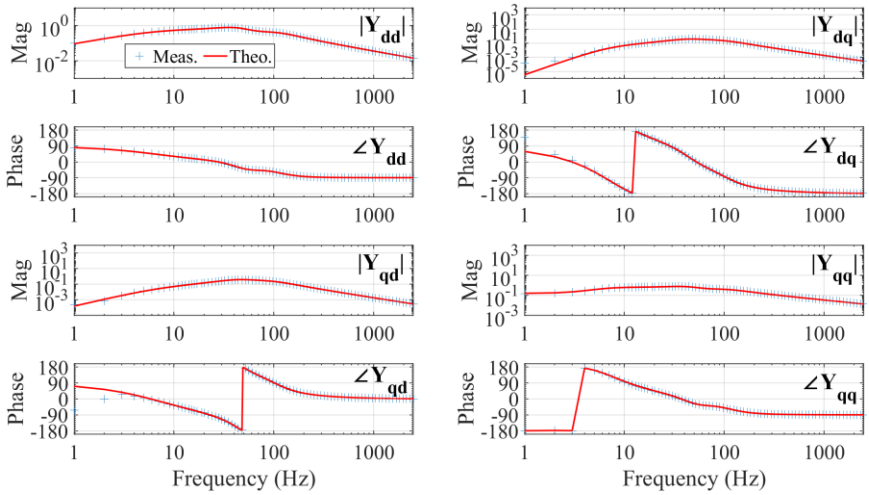

(b) PLL parameters $K_{\mathrm{pPLL}} = 60, K_{\mathrm{iPLL}} = 1800$

To further validate these results, additional benchmarking was performed with a frequency scanning tool addon to PSCAD™ developed by Manitoba Hydro Internation (MHI). The tool showed close alignment with results obtained using FAST. Further details can be found in Appendix A1.5.

3.1.3 Frequency scan in low frequency range

As mentioned in Section 3.1.2, discrepancy in the low-frequency range of dq- and qd-axis admittance components is observed. This section explores potential strategies to reduce this discrepancy.

Accuracy of the low frequency (below 3 Hz) measurements can be improved by adjusting the magnitude of the perturbation signal and the simulation time step. To do this, five frequency points (1, 2, 3, 4, and 5 Hz), are injected sequentially, rather than the multi-tone injection typically used in the PoC. The magnitude of each frequency component is increased from

0.125% to 5% of the steady-state PCC voltage magnitude. In addition, the simulation time step is decreased from 50 to 2 µs. The perturbation period is kept as 20 s.

Figure 9 shows the Bode plots of the theoretical and measured admittance frequency response using the FAST tool as the PLL parameters K_{pPLL} and K_{iPLL} are 60 and 1800, respectively, while the active current reference is 1.0 pu and the reactive current is 0 pu. In comparison to earlier Bode plots, the accuracy of Y_{dd} and Y_{qq} are not changed. However, in can be observed the accuracy of Y_{qd} has been significantly improved. The reason why Y_{dq} does not appear to be of the same level of accuracy as Y_{qd} is because its magnitude is very small, ($|Y_{dq}|$<10e-5, $|Y_{qd}|$~10e-4, $|Y_{dd}|$~$|Y_{qq}|$~10e-1). The off-diagonal elements are 0.01% of the diagonal elements in the low-frequency range.

Figure 9 Measured and theoretical admittance at IBR terminal for low frequency range

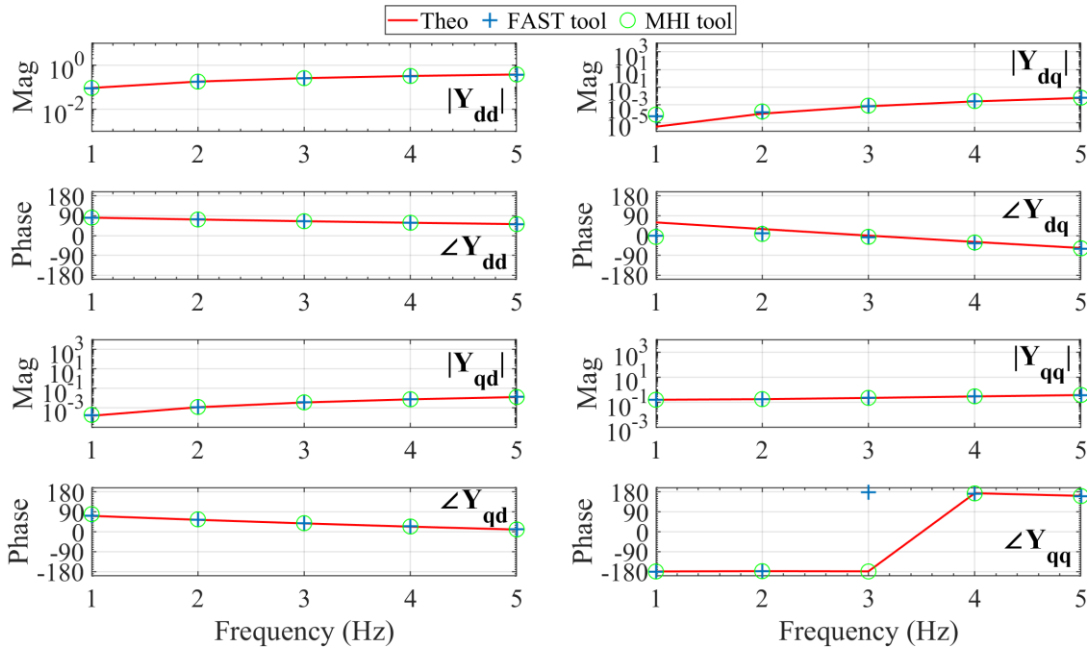

For benchmarking purposes, the admittance Bode plots measured using the MHI-developed tool are also presented in Figure 9. The perturbation configuration of the MHI tool is the same as that used by the FAST tool. Again, it is evident that both the FAST and MHI tools exhibit comparable performance in admittance measurement. Both methods can accurately capture the Y_{dd}, Y_{qd}, and Y_{qq} elements. Although a small discrepancy is observed between the theoretical and measured off-diagonal element Y_{dq} values. The Y_{dq} magnitude in this case is very small, which can be ignored.

Overall, the case studies show that the measurement accuracy of the two tools remains consistent and indicate that the accuracy in the low-frequency range can be improved by adjusting the configuration, such as perturbation magnitude, simulation step size and sequential frequency injection.

3.2 Black box IBR model

The white box model has permitted the development of a theoretical response that can now be used to check the measured response. The close alignment of measured and theoretical responses provides confidence in the frequency scanning technique to the point where it can be applied to a black box model.

The steps in the assessment are as follows:

1. Set up a SMIB model with varied grid conditions. In contrast to the white box model, the black box solar farm model includes the plant power controller (PPC) and other plant components.
2. Identify the total impedance at the connection point by perturbing the model and measuring the responses for a range of irradiances, operating conditions, SCR, and frequencies.
3. Analyse the results using frequency scan methods, such as Bode and Nyquist plots to assess the closed-loop stability for a range of irradiances, operating conditions and SCR and validate in EMT time domain simulations.

3.2.1 Model description

An existing site-specific solar farm model is used as the black box model for the assessment shown in Figure 10. The black box solar farm model includes the PPC and other plant components and is reflective of what would be analysed during a connection assessment process. Table 1 lists the parameters of the black box solar farm.

Figure 10 Black box IBR SMIB model diagram

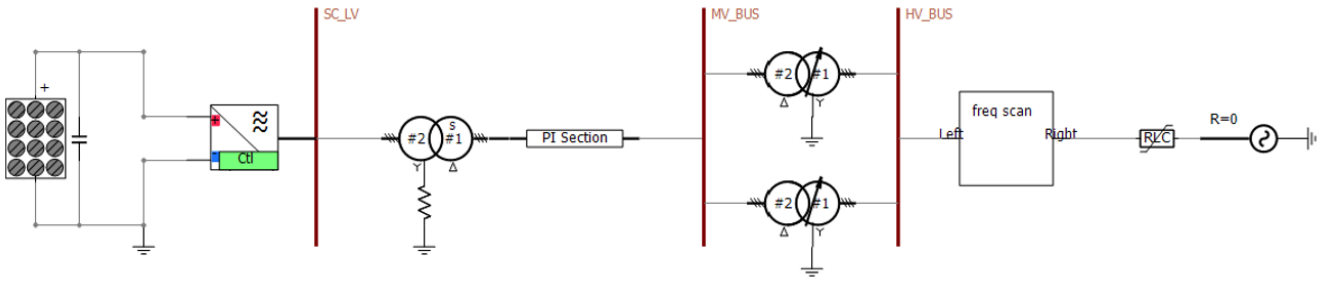

Table 1 Parameters of the black box solar farm model

Parameter	Value
Base voltage	66 kV
Base power	88 MW
Fundamental frequency	50 Hz
Base impedance	49.5 Ω
Base inductance	0.1575 H
Irradiance range	200 W/m^2-1000 W/m^2
Withstand SCR range	2-10

3.2.2 Generalized Nyquist Criterion and Bode Plot

The GNC is a robust stability assessment tool widely used in power systems. GNC extends the classical Nyquist stability criterion to multi-input multi-output (MIMO) systems by evaluating the eigenvalue loci of the open-loop transfer function in the complex plane. In the context of a grid connected IBR plant, GNC assesses the stability of the interconnected system by analysing the loop transfer function formed between the grid's admittance and the IBR's admittance.

The equivalent circuit of a SMIB model is shown in Figure 11 where the IBR is modelled as a Norton circuit equivalence and the grid is modelled as a Thevenin circuit equivalence. The grid current i_g can be calculated as:

$$i_g = \frac{Y_{\text{grid}}^{\text{matrix}}}{Y_{\text{ibr}}^{\text{matrix}} + Y_{\text{grid}}^{\text{matrix}}} I_{\text{ibr}} - \frac{Y_{\text{grid}}^{\text{matrix}} Y_{\text{ibr}}^{\text{matrix}}}{Y_{\text{ibr}}^{\text{matrix}} + Y_{\text{grid}}^{\text{matrix}}} V_{\text{grid}} = \underbrace{\frac{1}{1 + Y_{\text{ibr}}^{\text{matrix}} / Y_{\text{grid}}^{\text{matrix}}}}_{\text{Checking if having RHP poles}} \underbrace{(I_{\text{ibr}} - Y_{\text{ibr}}^{\text{matrix}} V_{\text{grid}})}_{\text{Stable}}$$

Since both the IBR and grid are assumed to be stable when operating independently, the second part of the last equation does not have any right-half-plane (RHP) poles. The stability of i_g is primarily determined by the first part of the equation, which reflects the interaction between the IBR's admittance and the grid's admittance. To assess this stability, two primary frequency domain methods are applied in this report, GNC plot and the Bode plot.

In the GNC plot, the traces of the two eigenvalues of measured impedance ratio $Y_{\text{ibr}}^{\text{matrix}} / Y_{\text{grid}}^{\text{matrix}}$ are mapped in the complex plane, and their behaviour with respect to the critical point (-1, j0) determines the system stability. If any of the eigenvalue loci encircle this point, it signifies the potential for instability in the closed-loop system.

For the Bode plot, the magnitude of the total impedance, $Z_{total} = 1/(Y_{\text{ibr}}^{\text{matrix}} + Y_{\text{grid}}^{\text{matrix}})$, should not exhibit any poorly damped peaks[12].

Figure 11 Equivalent circuit representation of the SMIB model

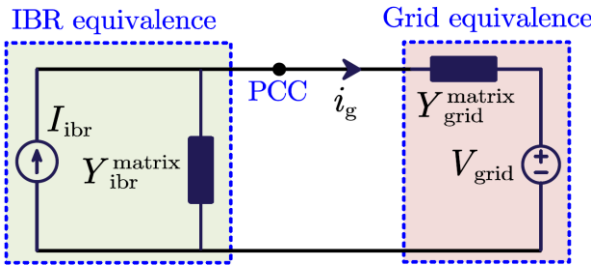

3.2.3 Approach

For the black box test, 337 frequency points logarithmically distributed between 6 and 45 Hz are selected for perturbation injection. The simulation step time should be set to 16.66667 µs. The initial phase shift for each frequency adopts the Schroeder multi-sine excitation style[13]. The perturbation time is 50 s to allow sufficient time for the lowest frequency of interest to complete enough cycles to reach a steady state.

A range of IBR operating scenarios is used to assess the accuracy of the scanning method. Those scenarios are classified into two cases:

- Stable cases: Investigates damped cases.
- Unstable cases: Investigates underdamped/undamped cases.

[12] Rygg Aet al. A modified sequence-domain impedance definition and its equivalence to the dq-domain impedance definition for the stability analysis of AC power electronic systems[J]. IEEE Journal of Emerging and Selected Topics in Power Electronics, 2016, 4(4): 1383-1396.

[13] Shibasaki Y et al. Analysis and design of multi-tone signal generation algorithms for reducing crest factor[C]//2020 IEEE 29th Asian Test Symposium (ATS). IEEE, 2020: 1-6.

The frequency scans are generated using the FAST tool. The admittance in the sequence-domain is used for the frequency scan analysis in this study. This facilitates the physical insights into the stability features in the positive- and negative-sequence domain. The transformation equation from dq-domain to sequence-domain is shown as follows:

$$Y_{\mathrm{ibr,pn}}^{\mathrm{matrix}} = A_{\mathrm{z}} Y_{\mathrm{ibr,dq}}^{\mathrm{matrix}} (A_{\mathrm{z}})^{-1},$$

where $A_z = \frac{1}{\sqrt{2}} \begin{bmatrix} 1 & j \\ 1 & -j \end{bmatrix}$.

3.2.4 Analysis and validation

The Bode plots are used to illustrate the total impedance of the IBR and the grid, as observed at the PCC. The Bode magnitude peak can reflect the dominant mode of the closed-loop system, composed of the IBR and the grid[14], which indicates the oscillating frequency. The accuracy of the frequency scanning results, especially the magnitude peak, can be verified by checking if there is a transient at this frequency in the time domain EMT simulations.

Stable case

Four scenarios in Table 2 are assessed under stable grid conditions.

Table 2 Stable black box model testing cases

Scenario	Irradiance (W/m²)	Active power (MW)	Reactive power (MVAr)	Tested SCR	X/R
1	250	20	0	10	4.9605
2	200	10	0	5	4.9605
3	800	70	0	4	4.9605
4	300	40	0	3	4.9605

Figure 12 shows the GNC plot with measured impedance ratio at PCC for scenario 1. The GNC plot shows that the loci of two eigenvalues are far away from the critical point (-1, j0), indicating a sufficient stability margin. The Bode plot of total impedance at PCC is presented in Figure 13. The Bode magnitude peak occurs at 19.9 Hz, indicating that the closed-loop system should have a 19.9 Hz dominant mode. The GNC plot provides visibility into the stability margin and Bode plot gives information on frequency of oscillation. The validation results for scenario 2 to 4 are presented in Appendix A2.1.

[14] W. Zhou, R. E. Torres-Olguin, M. K. Zadeh, B. Bahrani, Y. Wang, and Z. Chen, "Electromagnetic oscillation origin location in multiple-inverter-based power systems using components impedance frequency responses," IEEE Open Journal of the Industrial Electronics Society, vol. 2, pp. 1–20, 2020.

Figure 12 Stable case scenario 1, GNC plot of measured impedance ratio at PCC

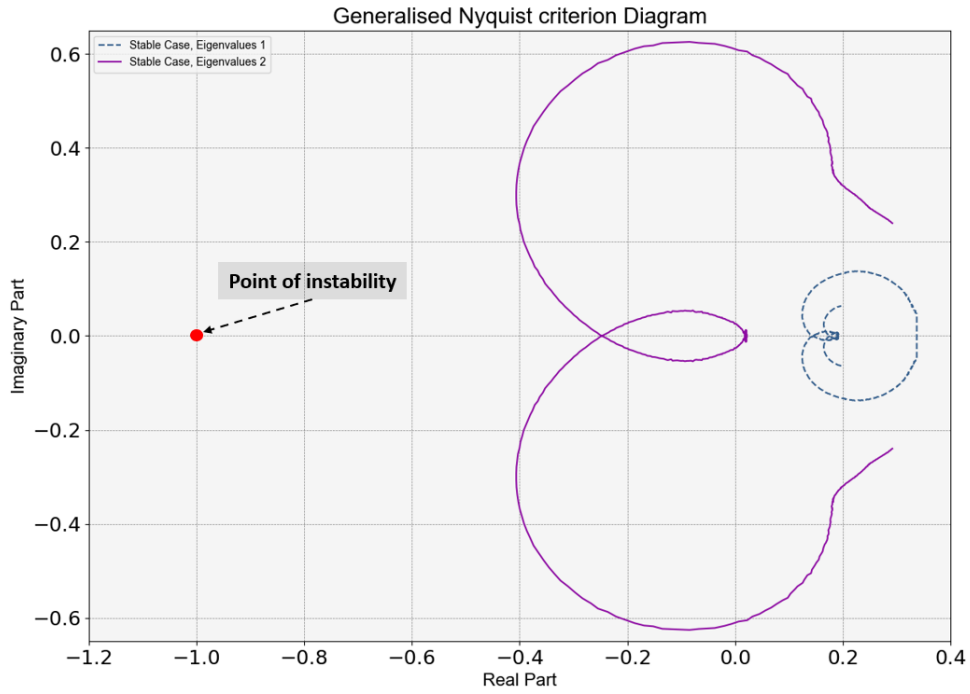

Figure 13 Stable case scenario 1, Bode plot of measured total impedance at PCC

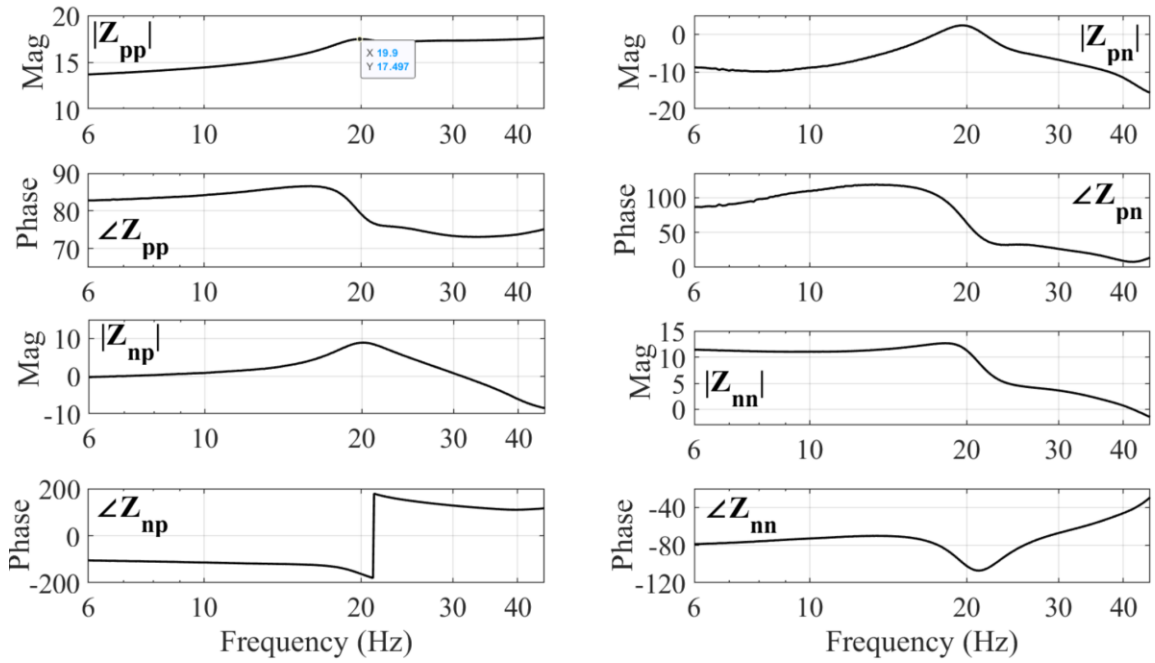

To excite the small-signal dynamics of the closed-loop system, a small variation in the grid impedance is applied at 40 s, that is for SCR step change from 15 to 10. Figure 14 shows the time domain waveforms of active power, reactive power, active current, and reactive current around 40 s. Figure 15 provides the FFT of the active and reactive currents from 40 to 50 s. A

transient waveform is observed at 19.3 Hz at t=40 s, which agrees with the 19.9 Hz magnitude peak, validating the ability of the frequency scanning tool to capture the closed-loop's small-signal dynamics.

Figure 14 Stable case scenario 1, time domain simulation results with SCR step change

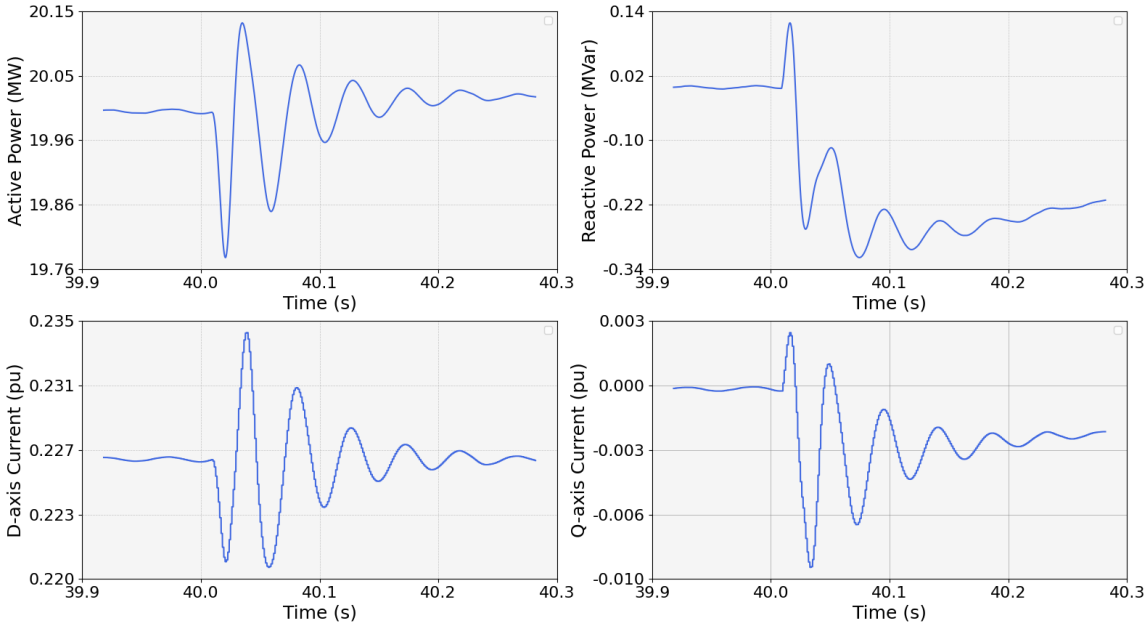

Figure 15 Stable case scenario 1, FFT results of the connection point current

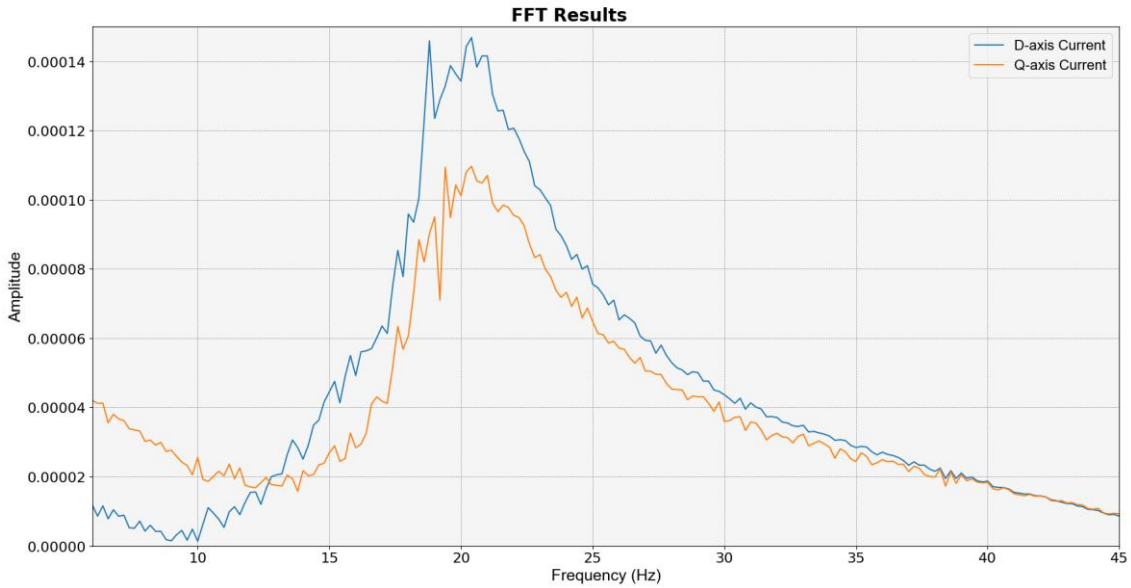

Unstable case

Five scenarios in Table 3 are assessed under weak grid conditions by changing the SCR to a value below three.

Table 3 Unstable black box model testing cases

Scenario	Irradiance (W/m²)	Active Power (MW)	Reactive power (MVAr)	Tested SCRs	X/R
1	300	40	0	[3.42, 2.63, 2.61, 2.55]	4.9605
2	270	40	0	[3.42, 2.63, 2.61, 2.55, 2.51]	4.9605
3	330	40	0	[3.42, 2.65, 2.63, 2.61]	4.9605
4	300	38	0	[3.42, 2.65, 2.63, 2.61]	4.9605
5	300	42	0	[3.42, 2.63, 2.61, 2.55, 2.51]	4.9605

Figure 16 shows the GNC plot of the impedance ratio at the PCC for scenario 1. The GNC plot is approaching the critical point (-1, j0) as the SCR decreases from 3.42 to 2.63 and then to 2.61, indicating degraded stability margin as the grid impedance increases. The GNC plot encircles the critical point at a SCR of 2.55, indicating the system is unstable under this grid condition. Furthermore, the Bode plot in Figure 17 indicates that the system may oscillate at 17 Hz under this grid condition.

Figure 16 Unstable case scenario 1, GNC plots of total impedance at the connection point with varied SCRs

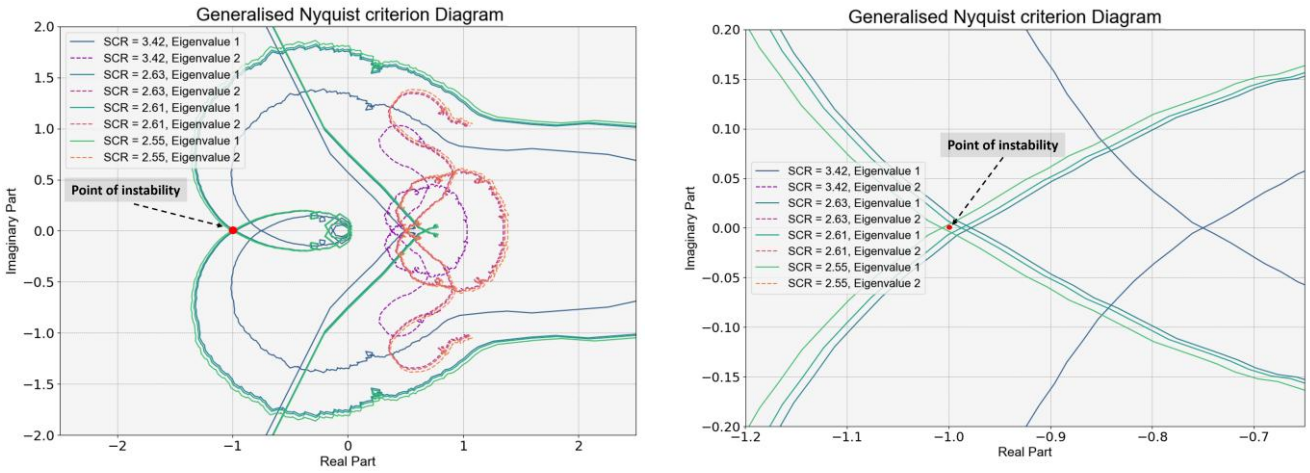

(a) Zoom out

(b) Zoom-in

Figure 17 Unstable case scenario 1, Bode plots of total impedance at PCC with varied SCRs

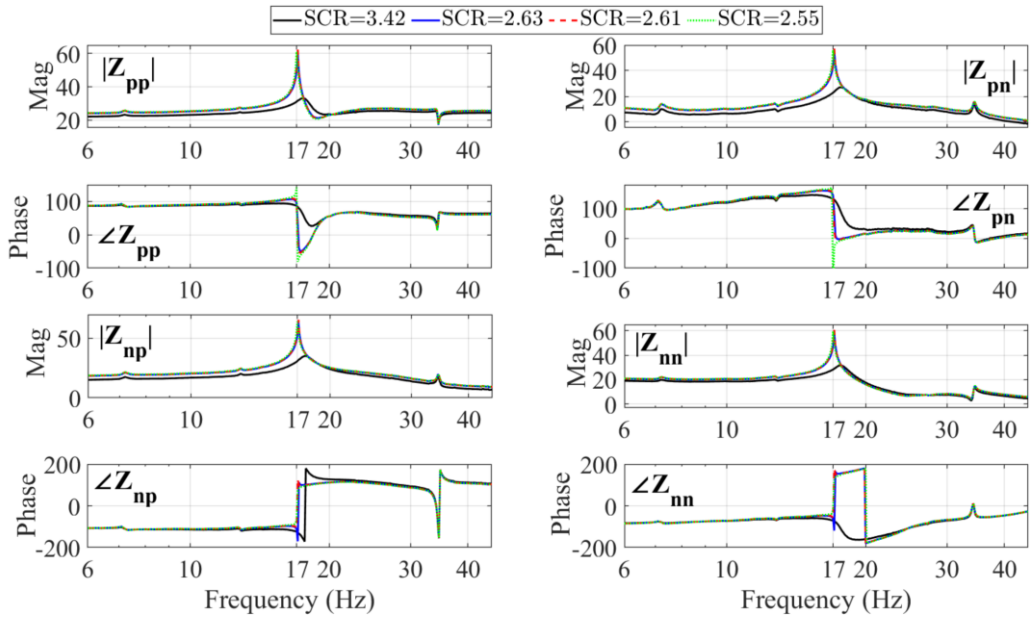

Figure 18 shows the EMT simulation results for scenario 1. The SCR is changed:

- From 3.42 to 2.61 at 40 s
- To 2.73 at 70 s.
- To 2.55 at 100 s.

As the figure demonstrates, it's evident that the system is initially stable, then marginally stable, stable again, and finally unstable under the above four grid conditions, which agrees with the frequency scan stability analysis. The figure shows that there are 17 periods from 40 s to 41 s, which agrees with the identified 17 Hz SSO in the Bode plot. Validation results for case 2 to 5 can be found in Appendix A2.2.

Figure 18 Unstable case scenario 1, time domain simulation results with varied SCRs

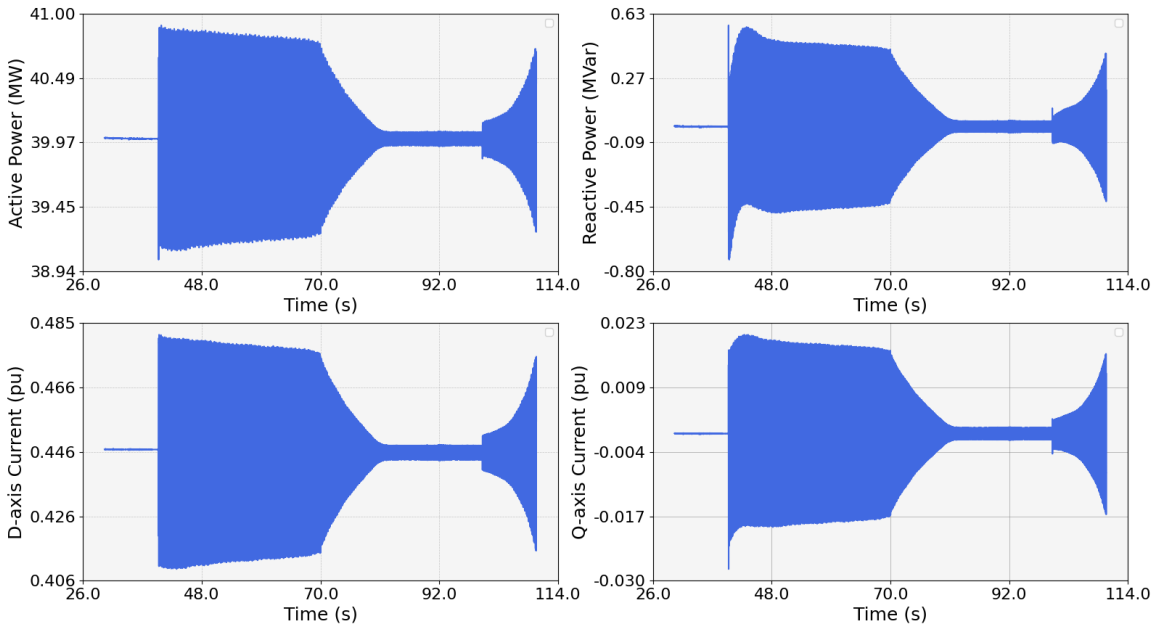

(a) Zoom-out

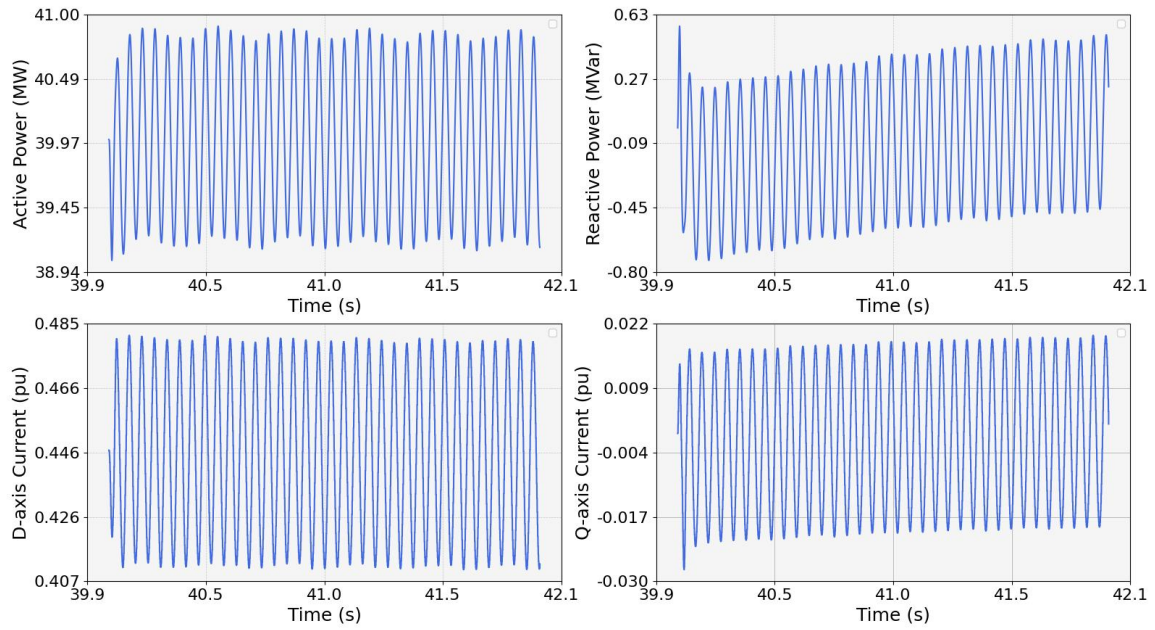

(b) Zoom-In at 40 s

4 Stage 2: Inverter-based resource controller tuning in SMIB model

In this section, the frequency scan method is used to adjust the controller parameters to improve the stability of the black box model used in Stage 1.

The controller design in the SMIB model will:

1. Identify the unstable condition of the IBR in weak grid conditions.
2. Obtain IBR admittance with varied control parameters via frequency scan at strong grid condition.
3. Calculate the impedance ratio at PCC under weak grid conditions with different control parameters.
4. Generate GNC plots for frequency-domain stability analysis.
5. Repeat step 3 and 4 until a sufficient stability margin is observed in GNC plots.
6. Validate performance in time domain simulation.

4.1 Analysis and validation

The same black box IBR model used in Stage 1 is assessed under weak grid conditions. Initial time domain simulations under this condition have shown an unstable response of the IBR. Following the steps mentioned above, the PLL parameters in the IBR are adjusted in the frequency domain to increase the damping factor until the plant is stable.

The GNC plot in Figure 19 shows the loci of two eigenvalues with three PLL controller damping ratios of 0.45, 0.75 and 1.05. The observation is summarised as follows:

- The loci of eigenvalue one with varied damping ratios extend to the right (positive side) of the real axis, indicating a very stable response.
- The loci of eigenvalue two are extending to the left of the real axis. These lobes approach and then encircle the (-1, j0) stability point.
- As the controller gain is increased, the magnitude of the ‘Eigenvalue 2’ lobes shrink, until a damping ratio of 1.05 results in this eigenvalue not encircling the instability point. The system is now marginally stable.

In practice, other controls could now be adjusted to further improve the damping and stability margins through an iterative process.

Figure 19 GNC plots with varied PLL damping ratios

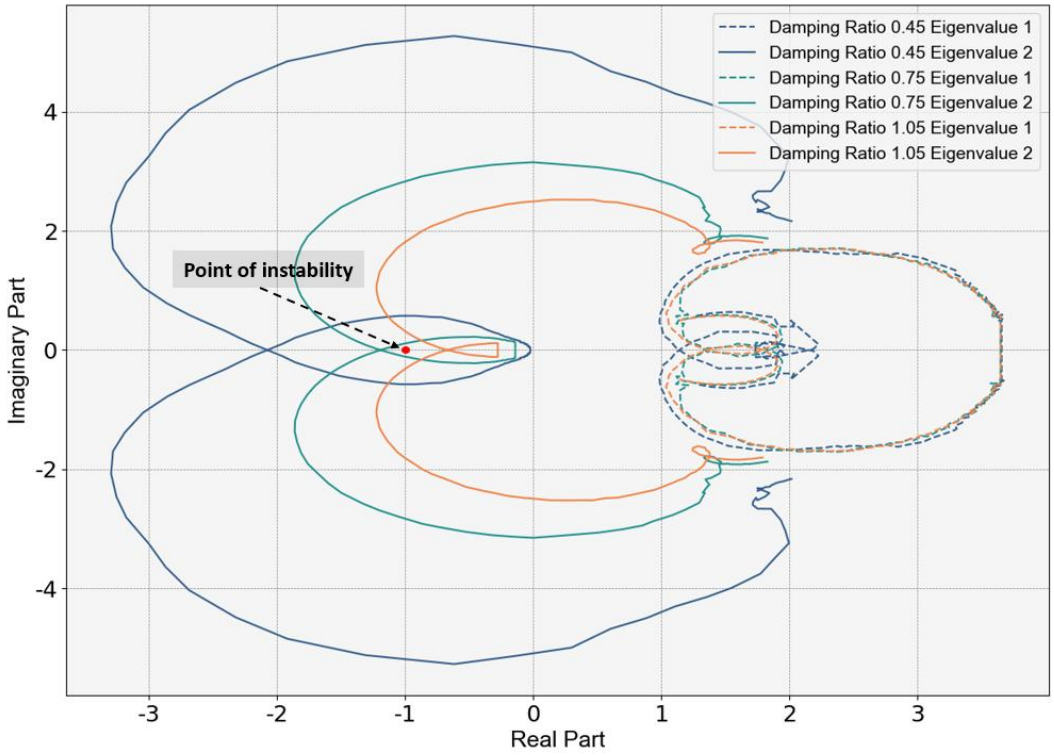

The time domain simulation results of the controllers analysed in the frequency domain are shown in Figure 20. A disturbance is introduced in the form of a step change in the SCR. The PLL damping ratio of 0.45 is unstable, damping ratio of 0.75 is marginally unstable and a damping ratio of 1.05 is marginally stable. These time domain simulation results agree with the GNC results, demonstrating the validity of the frequency scan method.

Figure 20 Time domain simulation results with varied PLL damping ratios

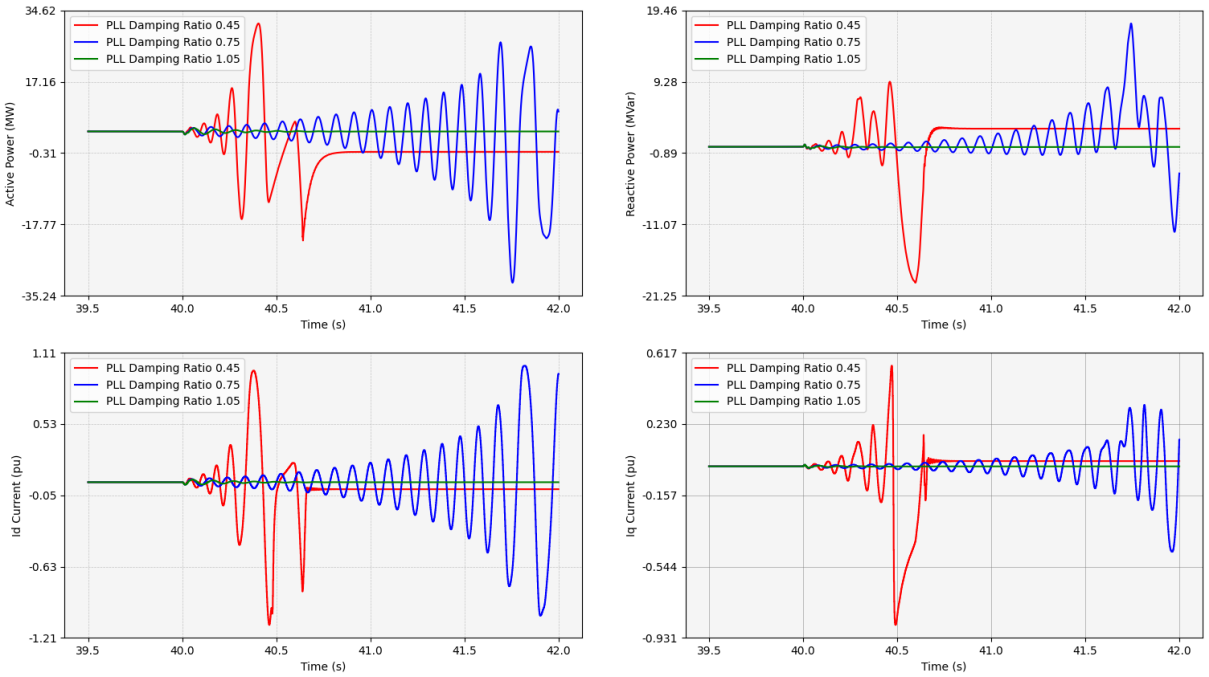

4.2 Summary

This section illustrates the ability to adjust controller settings for stability using frequency scan methods. The time domain simulations validate the frequency scan results, providing confidence the method yields reliable stability information over a wide frequency range.

In practice, large disturbances in the time domain can alter the system and controller behaviour as a result of nonlinear effects. However, if the power system survives the large disturbance, it will return to a stable operating point if the small signal analysis indicates stable operation.

Importantly, the frequency scan method will help identify instabilities or lightly damped performance over a wide range of frequencies, contributing to mitigating situations where sub-synchronous oscillations arise under certain operating conditions.

In this section, controller tuning efforts were primarily focused on adjusting the parameters of the PLL. While this approach is appropriate for demonstrating the technical feasibility of frequency scan-based analysis, it is important to acknowledge that OEMs do not generally permit proponents to modify PLL parameters.

To ensure the outcomes of this work remain relevant to real-world applications, the next stage of the proof of concept will investigate alternative controller parameters that proponents are typically permitted to tune. This aims to demonstrate how frequency scan techniques can support practical tuning decisions during the connection process.

5 Stage 3: Inverter-based resource controller design in wide area model

In this section, the IBR controller design in Stage 2 is further investigated to tuning the controller using the wide area EMT model. This is more representative of a real-world scenario for connecting IBR systems as it introduces the complexity of multiple neighbouring IBR systems, increasing the probability of interactions.

5.1 Approach

This stage describes the controller design for a new IBR connecting to a weak part of the power network using the wide area EMT model. The wide area EMT model includes all committed and operational generators in the NEM and is used to analyse potential interactions between the new IBR system and the existing systems connected in proximity to the connection point. The following steps were taken:

1. Consideration of the connection of the new IBR and identification of unstable operating scenarios.
2. Obtain the grid side admittance without the new IBR via a frequency scan at the connection point for unstable operating scenarios that include the new IBR.
3. Under the same IBR operating conditions giving unstable performance, obtain the IBR side admittance via frequency scan at the connection point in a SMIB model and with different control parameters. The SCR used in the SMIB model should ensure the IBR is in stable operation.
4. Combine the grid and IBR admittances to give the impedance ratio and total impedance at the connection point with different control parameters (equation can be found in Section 3.2.2). This gives one impedance per set of controller settings.
5. Generate GNC plots and Bode plots for frequency-domain stability analysis and provide guidance as to how to tune the control system for stability.
6. Validate performance in the time domain simulation.

5.1.1 Wide area EMT model

Stage 3 validation studies are conducted using an EMT model of an existing operational network where the solar farm plant from the previous stages is connected. The solar farm is located in a known low system strength area, owing to low synchronous fault levels due to its remoteness from major synchronous generators. Undamped oscillations were identified under certain operating scenarios. Figure 21 shows the single-line diagram of the neighbouring network configuration for the proposed connection of IBR1.

Figure 21 The neighbouring network configuration of the IBR1

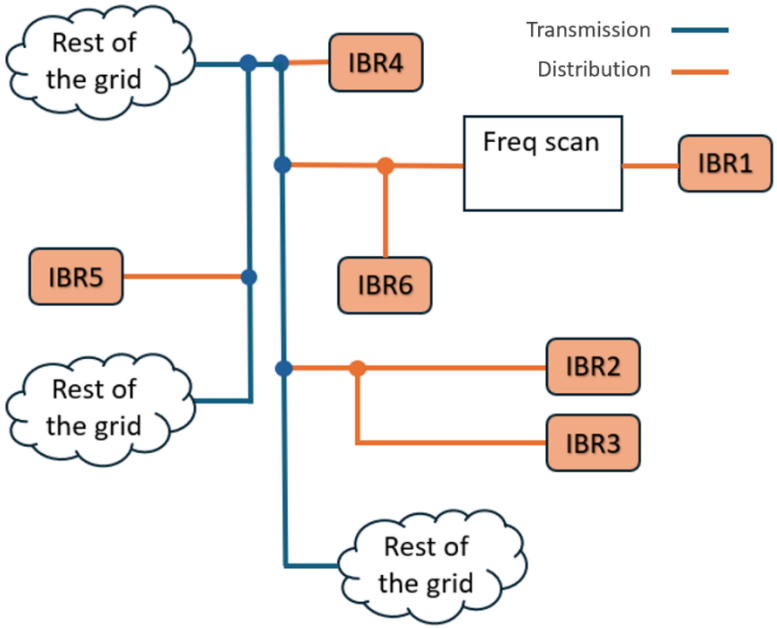

5.2 Analysis and validation

An operating scenario was identified through a series of simulations conducted under various operating conditions. Figure 22 shows how the new IBR1 is connected to the network at 10 s. The system starts undamped oscillations after connection, and IBR1 is subsequently tripped at 11 s. The first eight seconds are the initialisation period of the EMT simulation, and the relevant information is from this point onward. There are five other IBRs in the vicinity, and each of these is plotted in the diagrams. It can be observed that the connection of IBR1 is unstable and sets up unstable oscillations in other IBRs.

Figure 22 Time domain simulation results with untuned IBR1 plant

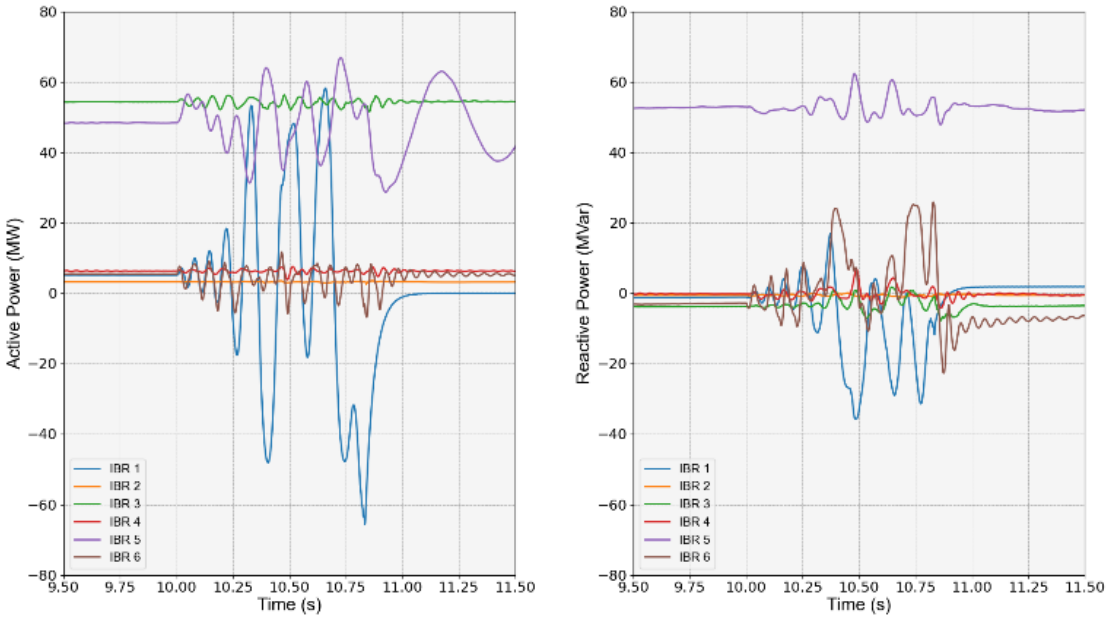

The goal of Stage 3 is to find controller parameters using the frequency scan method that will enable IBR1 to connect in a stable manner. As mentioned in Section 5.1, the frequency scan method and validation are conducted in above steps.

The GNC plot of the impedance ratio is shown in Figure 23. It can be observed that the GNC plot encircles the critical point (-1, j0), indicating an unstable system which aligns with the time domain simulation results from Figure 22. The Bode plot of total impedance at the connection shown in Figure 24 and shows poorly damped peaks of around 17 Hz. Fewer frequency points at only integer points (i.e. 1,2,3,4 Hz…) are used in this frequency scanning to obtain clear eigenvalue traces for a wide area model for shorter frequency scanning time.

Figure 23 GNC plots of impedance ratio at PCC with untuned IBR1 plant

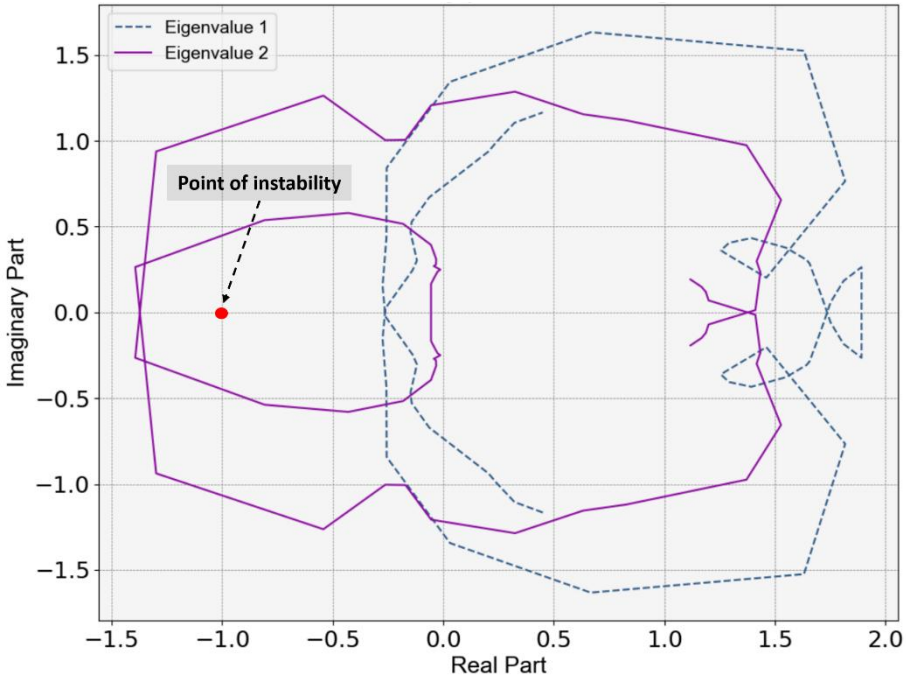

Figure 24 Bode plot of measured total impedance at PCC with untuned IBR1 plant

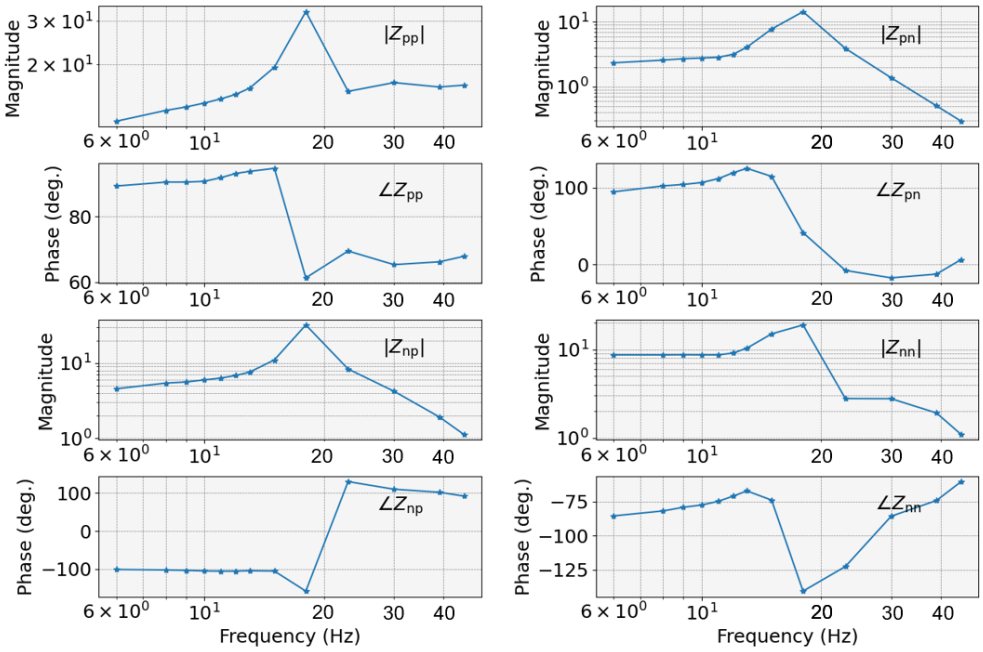

After validating the unstable response using frequency scan methods, the task is to tune IBR1 so that it can connect and remain stable. To achieve this, the IBR side admittance was recalculated with adjusted controller parameters. Combining the previously measured grid side admittance with the impedance ratio and the total impedance at the connection point, the values were then updated accordingly.

This is an iterative process, although not too time consuming as the IBR1 admittance is calculated in a SMIB model and the grid side admittance is unchanged. As shown in Figure 25, the GNC plot moves away from the critical point when improved settings are applied until a point is reached where the system is stable – that is, it no longer encircles the stability point (-1, j0). This is validated in Figure 26 where poorly damped peaks are no longer present.

In this final case, the GNC plot shows good gain and phase margins as the locus of eigenvalue two is now well clear of the instability point. It is also important to recognise that this analysis applies to only one power system operating scenario. There may be other operating scenarios where the gain and phase margins are different. It is important here to examine multiple operating scenarios that reflect the most realistic challenging power system conditions.

Figure 25 GNC plots of total impedance at the connection point with tuned IBR1 plant

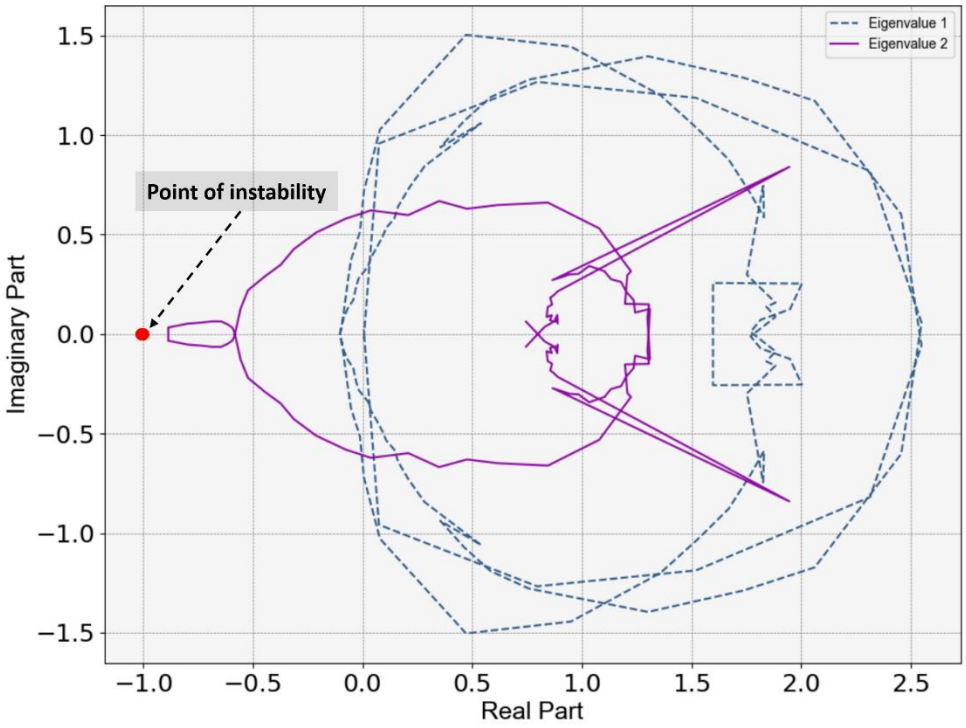

Figure 26 Bode plot of measured total impedance at PCC with tuned IBR1 plant

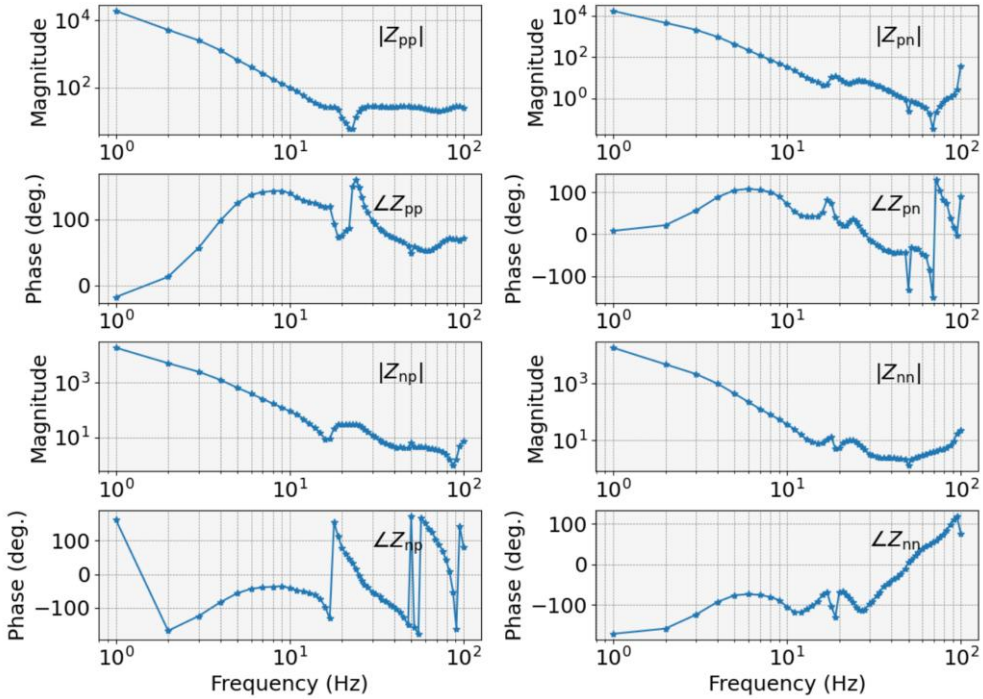

Following IBR controller retuning using the frequency scan method, the new controller settings are validated in time domain EMT simulations as shown in Figure 27. IBR1 is successfully connected to the wide area EMT model at 10 s with a small and damped oscillation. The response of IBR6 is relatively lightly damped by comparison but is still stable. In practice, there is

likely to be a benefit in re-examining the controller setting for IBR6 to see if the stability can be further improved and to test whether this oscillatory response occurs when IBR1 is not connected. For this report, stable operation after retuning IBR1 has achieved the goal of proof of concept. Therefore, further investigation of IBR6 is not investigated in this report.

Figure 27 Time domain simulation results with tuned IBR1 plant

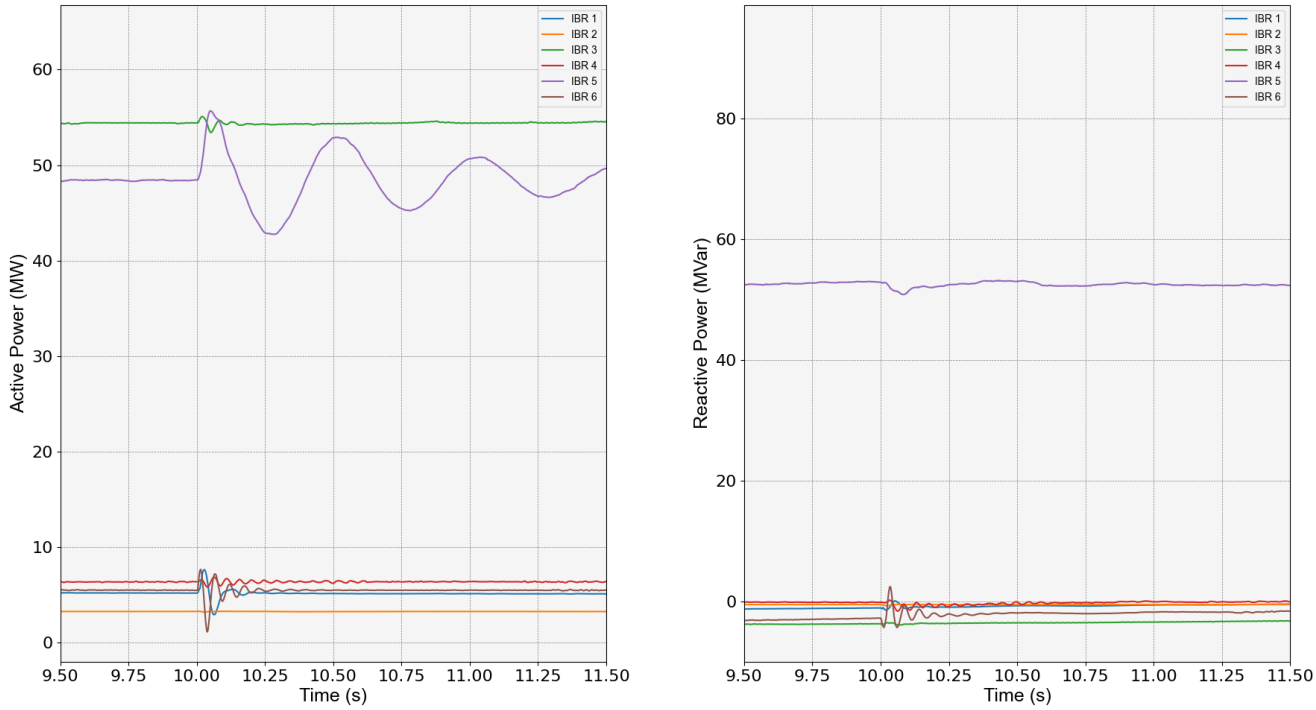

5.3 Summary

In Stage 3, the frequency scan method was used with the wide area EMT model to tune IBR1 controller. This analysis, when compared with the SMIB approach, adds significant complexity due to the neighbouring IBRs. The IBR1 controller parameters were adjusted to stabilise the response, allowing it to connect and operate under challenging conditions.

The analysis of the operating scenario using the GNC confirmed the stability issues occur because of the encirclement of the critical stability point (-1, j0). Working in the frequency domain using frequency scans of IBR1 obtained from a SMIB model, a controller was designed to give improved stability margins.

The frequency scan analysis of the wide area model with the revised controller showed a significant improvement in stability. This was validated in a time domain wide area EMT simulation, where the IBR1 was found to connect and operate in a stable manner.

In practice, several operating scenarios would be considered to test the sensitivity of the controller settings over the expected range of normal and extreme operating conditions to which IBR1 may be subjected. The time required to generate a frequency scan was observed to be comparable to a typical time domain EMT study. AEMO would expect a minimum of 5 operating scenarios to be studied to ensure a robust tuning is obtained.

6 Discussion and conclusions

Stage 1

The white box validation highlights complexities in the physics of the IBR plant, such as cross coupling between the d and q-axis or between positive and negative sequence reference frames. This leads to challenges in visualising and interpreting the results. However, the frequency scan method can clearly provide information about the stability of the generating system under assessment.

The frequency scans are derived by measuring responses in EMT simulations resulting from small voltage perturbations and analysing results with frequency scan method. Comparing the theoretical and measured results in a series of Bode plots shows:

- Close alignment is achieved between the theoretical results and the individual measurements for each frequency.
- A slight deviation between theoretical and measured results at low frequencies, below 3 Hz. The deviations between theoretical and measured results at low frequencies are inconsequential for purposes of controller tuning but may be relevant in other applications.
- Similar accuracy is obtained when model parameters are varied, indicating robustness for the scanning process and providing confidence in the technique.

For the black box IBR model validation, frequency scan techniques were used to adjust the parameters of the model to obtain a marginally stable and marginally unstable response. These adjustments in the frequency domain to achieve a marginally stable and marginally unstable system translate well in the time domain, exhibiting the expected performance.

The points of instability located in the frequency scans and time domain EMT studies closely align, reflecting the accuracy of the method. The results confirm that the frequency scanning method can accurately identify the stability boundary and resonance frequency of the black box IBR under various SCR conditions.

Stage 2

This analysis demonstrates the capability of the frequency scan method to assess the stability of a real IBR model when connected to a SMIB representation of the power system and to adjust PLL damping parameters to achieve a satisfactory level of stability. Conventional control system methods, using Nyquist and Bode plots, are used to provide a clear visual representation of the design process and the transition from unstable to stable behaviour.

While this approach is appropriate for demonstrating the technical feasibility of frequency scan-based analysis, it is important to acknowledge a key limitation: in typical connection processes, OEMs generally do not permit proponents to modify PLL parameters and any changes would require their consent.

Stage 3

Stage 3 extends the application of the frequency scan method to analysis of a new IBR connecting to a wide area network environment. The frequency scan method demonstrated the ability for the IBR controller to be tuned while considering the complex dynamics of neighbouring IBR systems and using a relatively small number of wide area time domain EMT studies. This method provides an advantage over the current time domain approach where multiple EMT simulations must be rerun

every time a parameter is tuned to confirm the performance over the entire range of operating scenarios. It remains necessary to evaluate various power system operating conditions to ensure that a set of parameters maintains stability under all scenarios. However, using frequency scanning can decrease the time required to tune IBR control systems and provide additional assurance regarding system stability.

A practical rule of thumb is that a minimum of 5 distinct power system operating scenarios should be sufficient to assess the performance of the IBR for the reasonably expected operating conditions. It should be noted the marginal benefit tends to diminish with additional cases, though the modelling and simulation effort per case study is constant. Based on this, critical operating scenarios can be identified, including high and low load, high and low irradiance, as well as N-1 outage. A frequency scan can be conducted in the wide area for each condition, with subsequent controller tuning taking place in a SMIB model. It is expected that the focus of the controller tuning may be further narrowed to the single most challenging scenario.

The frequency scan is performed via time domain simulation, by injecting a small perturbation and observing the response. Hence, the overall turnaround time is dictated by how quickly the time domain simulation can be run. As IBR controller tuning is performed using the SMIB model configuration, each IBR frequency scan was completed in approximately four minutes. Considering only the worst-case grid-side scan using the wide area model is required for tuning, the total setup and scan time remain manageable.

7 Next Steps

Based on the successful outcomes obtained from Stages 1 to 3 of the PoC, it is recommended that Stage 4 proceeds and that up to four live industry projects be analysed in conjunction with the relevant NSPs, Proponents and the OEM, if applicable.

By utilising live industry projects, Stage 4 will provide practical experience in applying and using frequency scan techniques and offer further insights into how these techniques can be incorporated into the connection process.

Appendix

A1. White box IBR model

A1.1 White box model description

The IBR block is a system of multiple sub-systems, including PLL, inverter and current controller as illustrated in Figure 28. The PPC module is not included in the simulation case as a single inverter system is used. The controller references for direct- and quadrature-axis currents are supplied manually.

Figure 28 IBR system internal modules

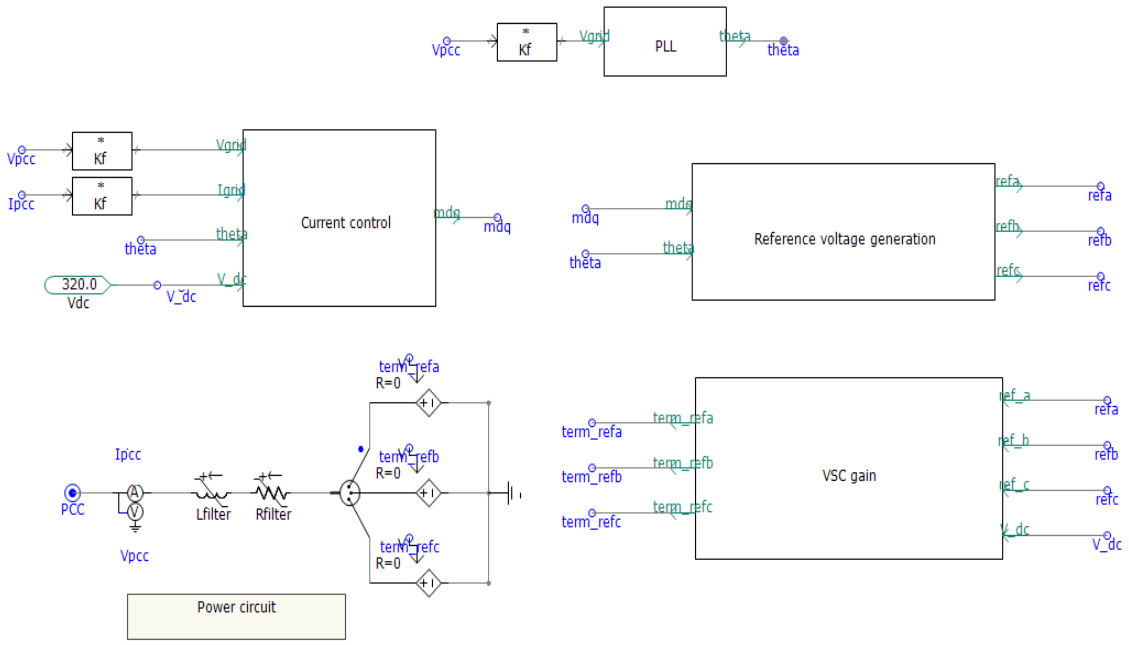

The description of each internal module in the IBR block is listed below:

- The PLL module receives three-phase voltages at the PCC as inputs and calculates the phase angle for the waveform through standard abc to dq0 conversion. The phase angle is then sent to the current control and reference voltage calculation block.
- The current control loop, based on the measured PCC voltage and current, determines reference signals for voltage in the d and q frames according to the desired current references for the d- and q-axis, defined inside the current control block. In the context of a power plant application, these references will be provided by the PPC.

- The reference voltage in the dq reference frame is then converted to the abc frame using the phase angle generated by the PLL. The reference voltage signals are then transmitted to the controlled voltage source via a simple average voltage source converter (VSC) gain block to generate the terminal voltage of the inverter..
- The power circuit consists of a resistor inductor (RL) filter that filters the harmonic components. The parameter value for the R filter and the L filter is defined in Appendix A1.2.

The white box model has internal components that are visible and can be analysed to give theoretical results. This enables the determination of output responses for given inputs. Figure 29 shows the internal structure of the IBR model adopted from the literature[15], with block diagrams of the Alternating Current Controller (ACC) and the PLL. In the figure:

- The ACC is equipped with cross-decoupling capability and a PCC voltage feed-forward path using a coefficient γ_{acc}.
- Two low-pass filters (LPFs) in the ACC module with time constants T_{i} and T_{v} are used to filter out high-frequency measurement noises of the grid current and PCC voltage.
- The Synchronous-Reference-Frame (SRF)-PLL is used to align the phase angle of the injected current with the PCC voltage.
- The dynamics of the PLL are determined by the PI controller with gains K_p and K_i.
- The superscript c indicates that the variables are represented in the controller reference frame.

Figure 29 Single-line control structure of the white box IBR connected to a resistive-inductive grid

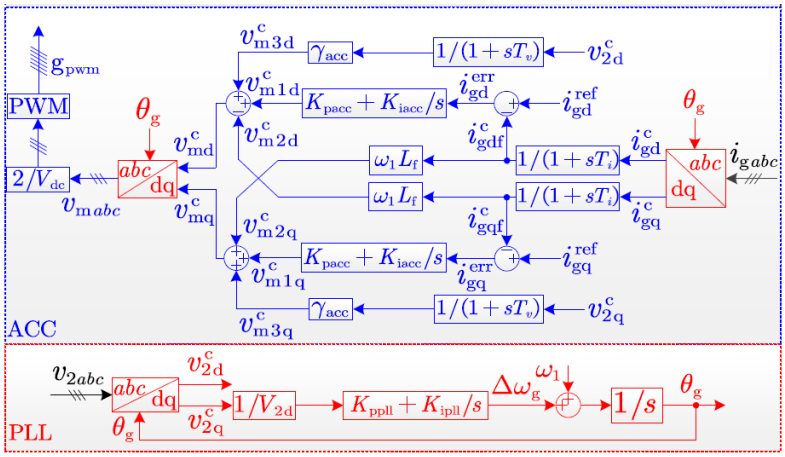

The theoretical state-space model of the white box IBR can be derived using the standard state-space representation as follows[16]:

$$\Delta\dot{\overrightarrow{x_{\mathrm{ibr}}}} = A_{\mathrm{ibr}}\Delta\overrightarrow{x_{\mathrm{ibr}}} + B_{\mathrm{ibr}}\Delta\overrightarrow{u_{\mathrm{ibr}}}$$
$$\Delta\overrightarrow{y_{\mathrm{ibr}}} = C_{\mathrm{ibr}}\Delta\overrightarrow{x_{\mathrm{ibr}}} + D_{\mathrm{ibr}}\Delta\overrightarrow{u_{\mathrm{ibr}}},$$

[15] Zhou W et al. Voltage and Current Dynamics Cancellation of Weak-Grid-Tied Grid-Following Inverters for Maximum Transferable Power Improvement[J]. IEEE Transactions on Energy Conversion, 2024, 39(3): 2053 - 2067.

[16] Zhou W et al. Comprehensive modelling, analysis, and comparison of state-space and admittance models of PLL-based grid-following inverters considering different outer control modes[J]. IEEE Access, 2022, 10: 30109-30146.

where:

- $\overrightarrow{u_{\text{ibr}}} = [v_{2,\text{d}}; v_{2,\text{q}}]$ is the input vector of PCC voltage in the dq reference frame;
- $\overrightarrow{y_{\text{ibr}}} = [i_{\text{g,d}}; i_{\text{g,q}}]$ is the grid current in the dq reference frame.

Appendix A1.3 provides the state-space matrices and dq-domain admittance model derivation.

A1.2 Model parameters

Table 4 Circuit and controller parameters of the white box IBR model

Parameter	Value
DC-link voltage V_{dc}	320 V
Grid fundamental frequency ω_1	100π rad/s
Filter resistance R_{f}	185.6 mΩ
Filter inductance L_{f}	4.45 mH
Switching frequency f_{swit}	10 kHz
Sampling frequency f_{samp}	10 kHz
Grid RMS voltage (phase-to-phase) V_{g}	110 V
Voltage LPF time constant T_{v}	0.02 s
Current LPF time constant T_{i}	0.002 s
PCC voltage feed-forward coefficient γ_{acc}	0
Proportional gain of current controller K_{pacc}	1.6 Ω
Integral gain of current controller K_{iacc}	66.7326 Ω/s
Proportional gain of PLL K_{pPLL}	22 rad/(Vs)
Integral gain of PLL K_{iPLL}	242 rad/($V\text{s}^2$)

A1.3 State-space model

The state-space model of the inner current controller can be derived as:

$$\Delta\dot{\vec{x}_i} = A_i\Delta\vec{x}_{\text{i}} + B_i\Delta\vec{u}_i$$
$$\Delta\vec{y}_i = C_i\Delta\vec{x}_i + D_i\Delta\vec{u}_i,$$

where the symbol Δ denotes the small-signal perturbation $A_i = \mathbf{0}_{2\times 2}$, $B_i = [1,0;0,1]$, $C_i = [K_{ii},0;0,K_{ii}]$, and $D_i = [K_{pi},0;0,K_{pi}]$.

The state-space model of the time delay can be derived as:

$$\Delta\dot{\overrightarrow{x_{del}}} = A_{del}\Delta\overrightarrow{x_{del}} + B_{del}\Delta\overrightarrow{u_{del}}$$
$$\Delta\overrightarrow{y_{del}} = C_{del}\Delta\overrightarrow{x_{del}} + D_{del}\Delta\overrightarrow{u_{del}},$$

where

$$A_{del} = \begin{bmatrix} 0 & 1 & 0 & 0 & 0 & 0 \\ 0 & 0 & 1 & 0 & 0 & 0 \\ \frac{-120}{T_d^3} & \frac{-60}{T_d^2} & \frac{-12}{T_d} & 0 & 0 & 0 \\ 0 & 0 & 0 & 0 & 1 & 0 \\ 0 & 0 & 0 & 0 & 0 & 1 \\ 0 & 0 & 0 & \frac{-120}{T_d^3} & \frac{-60}{T_d^2} & \frac{-12}{T_d} \end{bmatrix}, \; B_{del} = \begin{bmatrix} 0 & 0 \\ 0 & 0 \\ 1 & 0 \\ 0 & 0 \\ 0 & 0 \\ 0 & 1 \end{bmatrix},$$
$$C_{del} = \begin{bmatrix} \frac{240}{T_d^3} & 0 & \frac{24}{T_d} & 0 & 0 & 0 \\ 0 & 0 & 0 & \frac{240}{T_d^3} & 0 & \frac{24}{T_d} \end{bmatrix}, \; D_{del} = \begin{bmatrix} -1 & 0 \\ 0 & -1 \end{bmatrix}.$$

The state-space model of the PLL can be derived as:

$$\Delta\dot{\overrightarrow{x_{pll}}} = A_{pll}\Delta\overrightarrow{x_{\mathrm{pll}}} + B_{pll}\Delta\overrightarrow{u_{pll}}$$
$$\Delta\overrightarrow{y_{pll}} = C_{pll}\Delta\overrightarrow{x_{pll}} + D_{pll}\Delta\overrightarrow{u_{pll}},$$

where $A_{pll} = [0, K_{ipll}; 0, 0]$, $B_{pll} = [K_{ppll}; 1]$, $C_{pll} = [1, 0]$, and $D_{pll} = 0$.

Combining the state-space models of current control, time delay, and PLL, the state-space model of the whole IBR can be derived as:

$$A_{\mathrm{ibr}}=\begin{bmatrix}
\frac{-1}{T_{\mathrm{i}}} & 0 & 0 & 0 & 0 & 0 & 0 & 0 & 0 & 0 & 0 & 0 & \frac{1}{T_{\mathrm{i}}} & 0 & 0 & 0 \\
0 & \frac{-1}{T_{\mathrm{i}}} & 0 & 0 & 0 & 0 & 0 & 0 & 0 & 0 & 0 & 0 & 0 & \frac{1}{T_{\mathrm{i}}} & 0 & 0 \\
0 & 0 & \frac{-1}{T_{\mathrm{v}}} & 0 & 0 & 0 & 0 & 0 & 0 & 0 & 0 & 0 & 0 & 0 & 0 & 0 \\
0 & 0 & 0 & \frac{-1}{T_{\mathrm{v}}} & 0 & 0 & 0 & 0 & 0 & 0 & 0 & 0 & 0 & 0 & -\frac{V_{2,\mathrm{d}}}{T_{\mathrm{v}}} & 0 \\
-1 & 0 & 0 & 0 & 0 & 0 & 0 & 0 & 0 & 0 & 0 & 0 & 0 & 0 & 0 & 0 \\
0 & -1 & 0 & 0 & 0 & 0 & 0 & 0 & 0 & 0 & 0 & 0 & 0 & 0 & 0 & 0 \\
0 & 0 & 0 & 0 & 0 & 0 & 0 & 1 & 0 & 0 & 0 & 0 & 0 & 0 & 0 & 0 \\
0 & 0 & 0 & 0 & 0 & 0 & 0 & 0 & 1 & 0 & 0 & 0 & 0 & 0 & 0 & 0 \\
-K_{\mathrm{pacc}} & -\frac{V_{\mathrm{dc}}w_1L_{\mathrm{f}}}{2} & \Upsilon_{\mathrm{acc}} & 0 & K_{\mathrm{iacc}} & 0 & \frac{-120}{T_{\mathrm{d}}^3} & \frac{-60}{T_{\mathrm{d}}^2} & \frac{-12}{T_{\mathrm{d}}} & 0 & 0 & 0 & 0 & 0 & 0 & 0 \\
0 & 0 & 0 & 0 & 0 & 0 & 0 & 0 & 0 & 0 & 1 & 0 & 0 & 0 & 0 & 0 \\
0 & 0 & 0 & 0 & 0 & 0 & 0 & 0 & 0 & 0 & 0 & 1 & 0 & 0 & 0 & 0 \\
\frac{V_{\mathrm{dc}}w_1L_{\mathrm{f}}}{2} & -K_{\mathrm{pacc}} & 0 & \Upsilon_{\mathrm{acc}} & 0 & K_{\mathrm{iacc}} & 0 & 0 & 0 & \frac{-120}{T_{\mathrm{d}}^3} & \frac{-60}{T_{\mathrm{d}}^2} & \frac{-12}{T_{\mathrm{d}}} & 0 & 0 & 0 & 0 \\
\frac{V_{\mathrm{dc}}K_{\mathrm{pacc}}}{2L_{\mathrm{f}}} & w_1 & -\frac{V_{\mathrm{dc}}\Upsilon_{\mathrm{acc}}}{2L_{\mathrm{f}}} & 0 & -\frac{V_{\mathrm{dc}}K_{\mathrm{iacc}}}{2L_{\mathrm{f}}} & 0 & \frac{120V_{\mathrm{dc}}}{L_{\mathrm{f}}T_{\mathrm{d}}^3} & 0 & \frac{12V_{\mathrm{dc}}}{L_{\mathrm{f}}T_{\mathrm{d}}} & 0 & 0 & 0 & -\frac{R_{\mathrm{f}}}{L_{\mathrm{f}}} & w_1 & 0 & 0 \\
-w_1 & \frac{V_{\mathrm{dc}}K_{\mathrm{pacc}}}{2L_{\mathrm{f}}} & 0 & -\frac{V_{\mathrm{dc}}\Upsilon_{\mathrm{acc}}}{2L_{\mathrm{f}}} & 0 & -\frac{V_{\mathrm{dc}}K_{\mathrm{iacc}}}{2L_{\mathrm{f}}} & 0 & 0 & 0 & \frac{120V_{\mathrm{dc}}}{L_{\mathrm{f}}T_{\mathrm{d}}^3} & 0 & \frac{12V_{\mathrm{dc}}}{L_{\mathrm{f}}T_{\mathrm{d}}} & -w_1 & -\frac{R_{\mathrm{f}}}{L_{\mathrm{f}}} & \frac{V_{2,\mathrm{d}}}{L_{\mathrm{f}}} & 0 \\
0 & 0 & 0 & 0 & 0 & 0 & 0 & 0 & 0 & 0 & 0 & 0 & 0 & 0 & -K_{\mathrm{ppll}} & K_{\mathrm{ipll}} \\
0 & 0 & 0 & 0 & 0 & 0 & 0 & 0 & 0 & 0 & 0 & 0 & 0 & 0 & -1 & 0
\end{bmatrix}$$

$$B_{\mathrm{ibr}}=\begin{bmatrix}
0 & 0 & 0 & 0 \\
0 & 0 & 0 & 0 \\
0 & 0 & \frac{1}{T_{\mathrm{v}}} & 0 \\
0 & 0 & 0 & \frac{1}{T_{\mathrm{v}}} \\
1 & 0 & 0 & 0 \\
0 & 1 & 0 & 0 \\
0 & 0 & 0 & 0 \\
0 & 0 & 0 & 0 \\
K_{\mathrm{pacc}} & 0 & 0 & 0 \\
0 & 0 & 0 & 0 \\
0 & 0 & 0 & 0 \\
0 & K_{\mathrm{pacc}} & 0 & 0 \\
-\frac{V_{\mathrm{dc}}K_{\mathrm{pacc}}}{2L_{\mathrm{f}}} & 0 & \frac{-1}{L_{\mathrm{f}}} & 0 \\
0 & -\frac{V_{\mathrm{dc}}K_{\mathrm{pacc}}}{2L_{\mathrm{f}}} & 0 & \frac{-1}{L_{\mathrm{f}}} \\
0 & 0 & 0 & \frac{K_{\mathrm{ppll}}}{V_{2,\mathrm{d}}} \\
0 & 0 & 0 & \frac{1}{V_{2,\mathrm{d}}}
\end{bmatrix},\qquad
C_{\mathrm{ibr}}=\begin{bmatrix}
0 & 0 & 0 & 0 & 0 & 0 & 0 & 0 & 0 & 0 & 0 & 0 & 1 & 0 & -I_{\mathrm{g,q}} & 0 \\
0 & 0 & 0 & 0 & 0 & 0 & 0 & 0 & 0 & 0 & 0 & 0 & 0 & 1 & I_{\mathrm{g,d}} & 0
\end{bmatrix},\quad
D_{\mathrm{ibr}}=\begin{bmatrix}
0 & 0 & 0 & 0 \\
0 & 0 & 0 & 0
\end{bmatrix}$$

where T_{d} represents the time delay.

Based on the equation above, the dq-domain admittance model can be derived as

$$Y_{\mathrm{ibr,dq}}^{\mathrm{matrix}}=-C_{\mathrm{ibr}}\left(sI_{16}-A_{\mathrm{ibr}}\right)B_{\mathrm{ibr}}-D_{\mathrm{ibr}}$$

where I_{16} is the 16th-order unit matrix.

A1.4 Frequency points for frequency scan

Table 5 80 frequency points for perturbation injection

Num	Freq (Hz)	Num	Freq (Hz)	Num	Freq (Hz)	Num	Freq (Hz)
1	1	21	24	41	115	61	557
2	2	22	26	42	124	62	603
3	3	23	28	43	134	63	652
4	4	24	30	44	145	64	706
5	5	25	32	45	157	65	764
6	6	26	35	46	170	66	827
7	7	27	38	47	184	67	895
8	8	28	41	48	199	68	968
9	9	29	44	49	216	69	1048
10	10	30	48	50	233	70	1134
11	11	31	52	51	253	71	1228
12	12	32	56	52	273	72	1328
13	13	33	61	53	296	73	1438
14	14	34	66	54	320	74	1556
15	15	35	71	55	347	75	1684
16	16	36	77	56	375	76	1822
17	17	37	84	57	406	77	1972
18	19	38	90	58	439	78	2134
19	20	39	98	59	476	79	2310
20	22	40	106	60	515	80	2500

A1.5 Frequency scanning tool benchmarking

To validate the accuracy of the admittance measurement using the FAST tool, the MHI-developed toolbox is tested as a benchmark. The configuration for the MHI tool is as follows:

- Scanned frequency range: 1 - 100 Hz with 1 Hz step (100 frequency point injected in two times).
- Perturbation magnitude: 0.125% of the steady-state PCC voltage per frequency component.
- Simulation step time: 50 microseconds (µs).
- Initial phase shift: determined by Schroeder multi-sine excitation.
- Perturbation duration: 20 s, allowing the lowest frequency to complete enough cycles to reach steady state.

Figure 30 presents the theoretical and measured admittance plots of the IBR when the PLL parameters are (60, 1800), with an active current reference of 1.0 pu and a reactive current reference of 0 pu. It is evident that both FAST and MHI tools accurately capture the diagonal elements. Although both tools show measurement discrepancies in the low-frequency

range for the off-diagonal elements, Y_{dq} and Y_{qd}. Overall, this benchmarking study suggests that the FAST tool performs comparably to the MHI-developed tool.

Figure 30 Measured and theoretical admittance at IBR terminal with FAST and MHI frequency scan tools

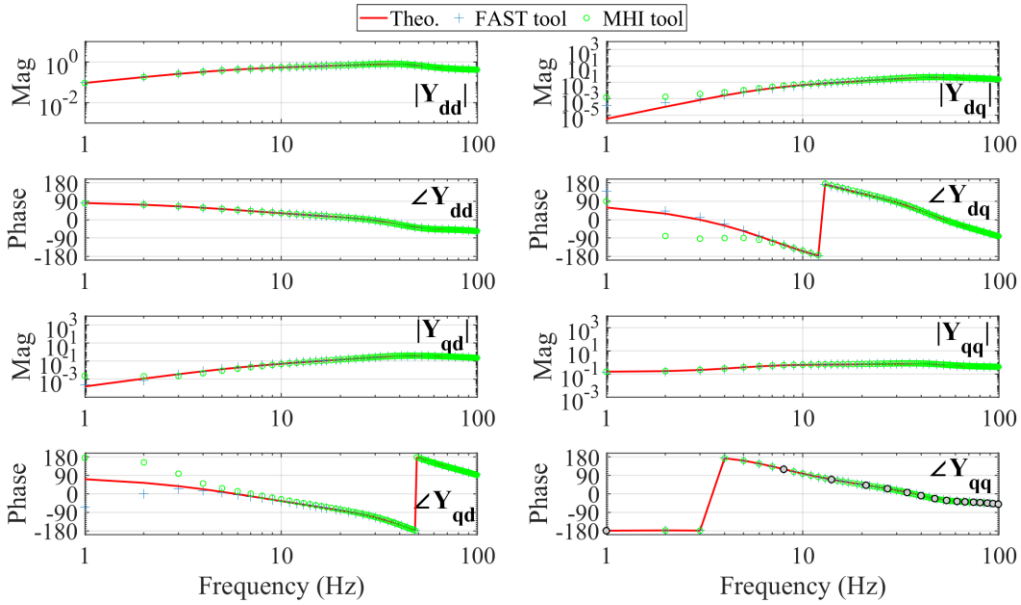

The observed discrepancy in the low-frequency range of dq- and qd-axis admittance components is discussed in section 3.1.3.

Additionally, the FAST tool was benchmarked against several other commercial and open-source tools. Overall, the FAST tool benchmarked well against these other tools and the results were presented at CIGRE Australia 2025[17].

[17] At: https://www.aemo.com.au/-/media/files/initiatives/frequency-scanning/benchmarking-of-six-different-frequency-scan-tools.pdf

A2. Black box IBR model validation

A2.1 Stable cases validation results

A2.1.1 Scenario 2

Figure 31 shows the GNC plot of measured impedance ratio at PCC for scenario 2. The GNC plot is closer to the critical point (-1, j0) compared to scenario 1, indicating a decreased stability margin. Figure 32 shows the Bode plot of total impedance at PCC. The Bode magnitude peak occurs at 18.5 Hz, indicating that the closed-loop system should have an 18.5 Hz dominant mode. Both GNC and the Bode plot for the complete system are analysed.

Figure 31 Stable case scenario 2, GNC plot of measured impedance ratio at PCC

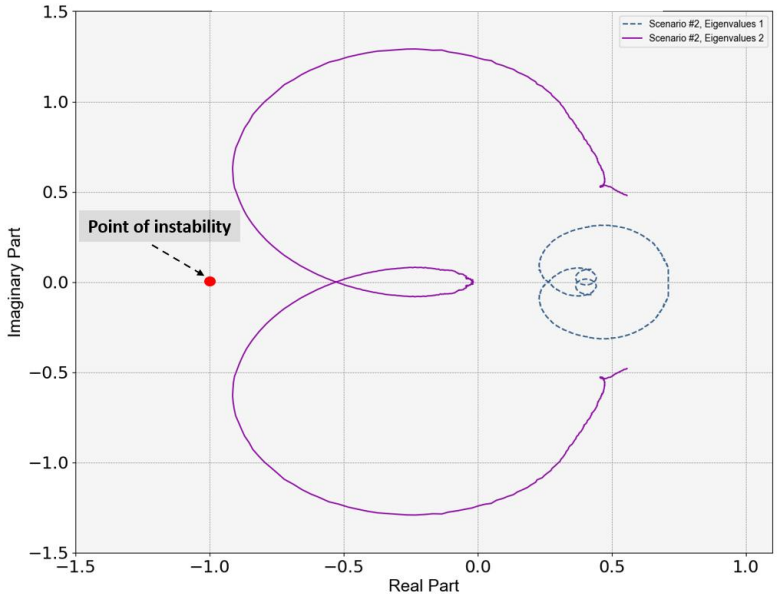

Figure 32 Stable case scenario 2, Bode plot of measured total impedance at PCC

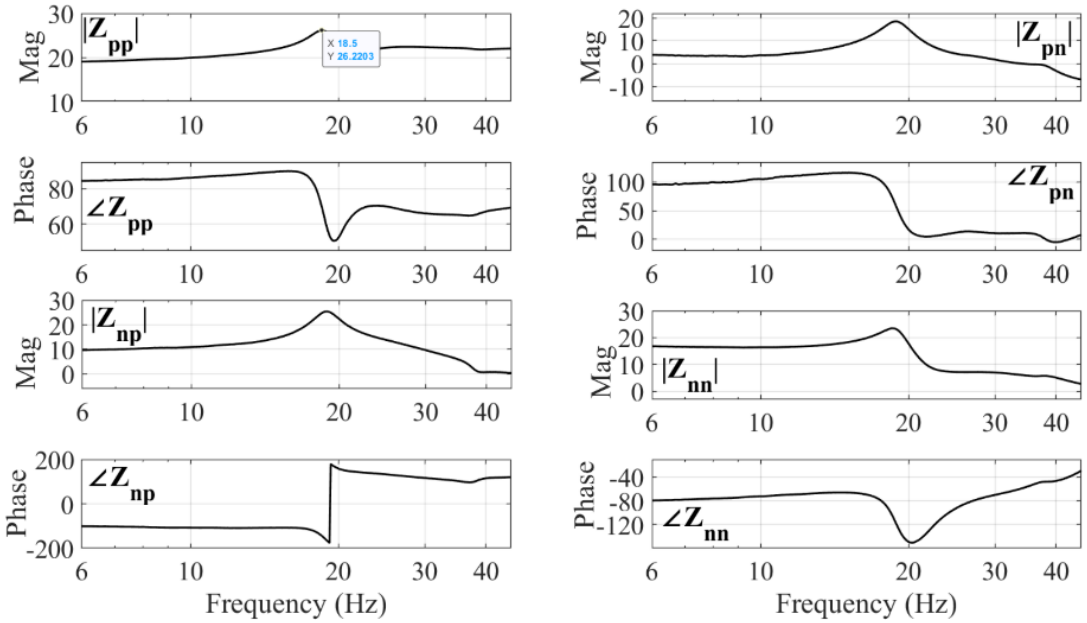

To excite the small-signal dynamics of the closed-loop system, a small variation in the grid impedance, SCR step change from 5.5 to 5, is applied at 40 s. Figure 33 shows the time domain responses of active power, reactive power, active current, and reactive current following this disturbance. The FFT of the active and reactive currents from 40 to 50 s is presented in Figure 34. The FFT shows a peak at 18.7 Hz at 40 s, which agrees with the 18.5 Hz magnitude peak shown in the Bode plot.

Figure 33 Stable case scenario 2, time domain simulation with SCR step change

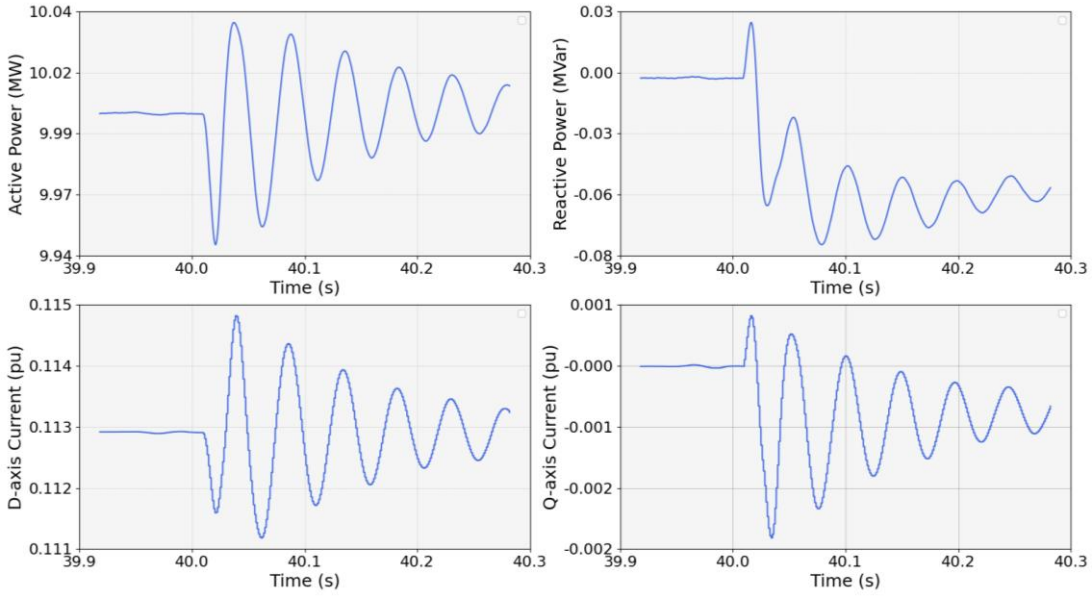

Figure 34 Stable case scenario 2, FFT results of the connection point current

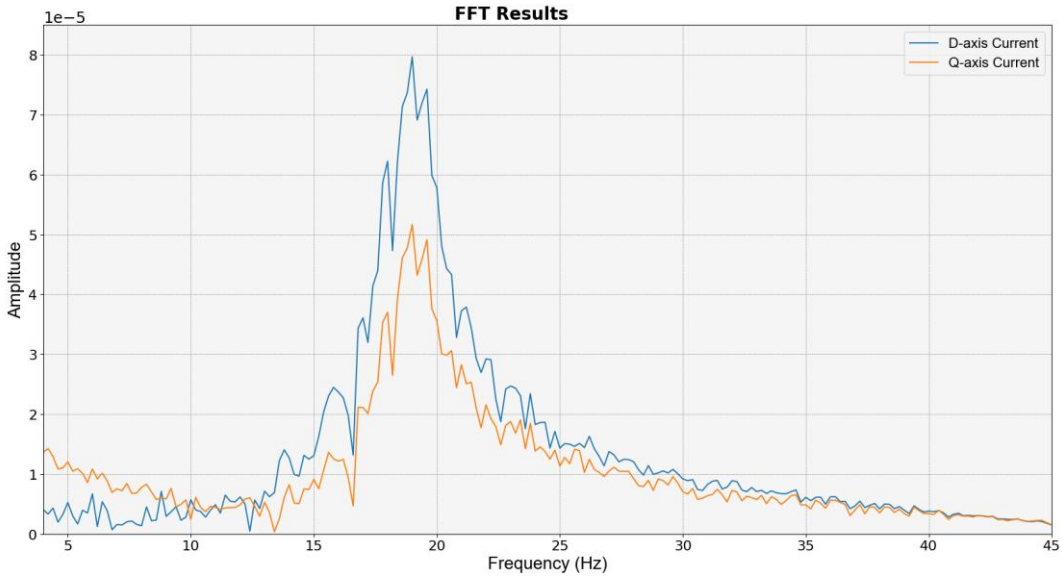

A2.1.2 Scenario 3

Figure 35 shows the GNC plot of the measured impedance ratio at PCC for scenario 3. The GNC plot is closer to the critical point (-1, j0) compared to scenario 2, indicating a decreased stability margin. Figure 36 shows the Bode plot of total impedance at the connection point. The Bode magnitude peak occurs at 17.9 Hz, indicating that the closed-loop system should have a 17.9 Hz dominant mode. Both the GNC and the Bode plot for the complete system are analysed.

Figure 35 Stable case scenario 3, GNC plot of measured impedance ratio at PCC

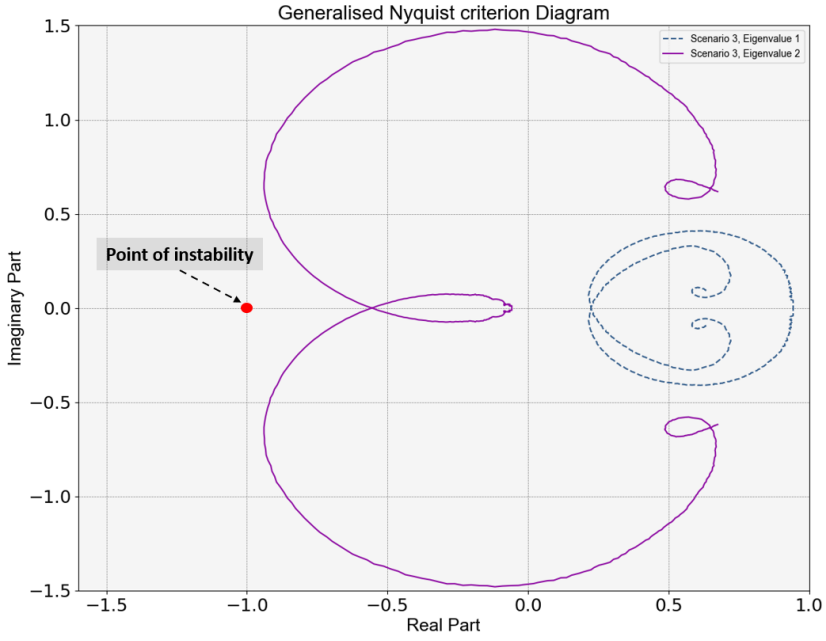

Figure 36 Stable case scenario 3, Bode plot of measured total impedance at PCC

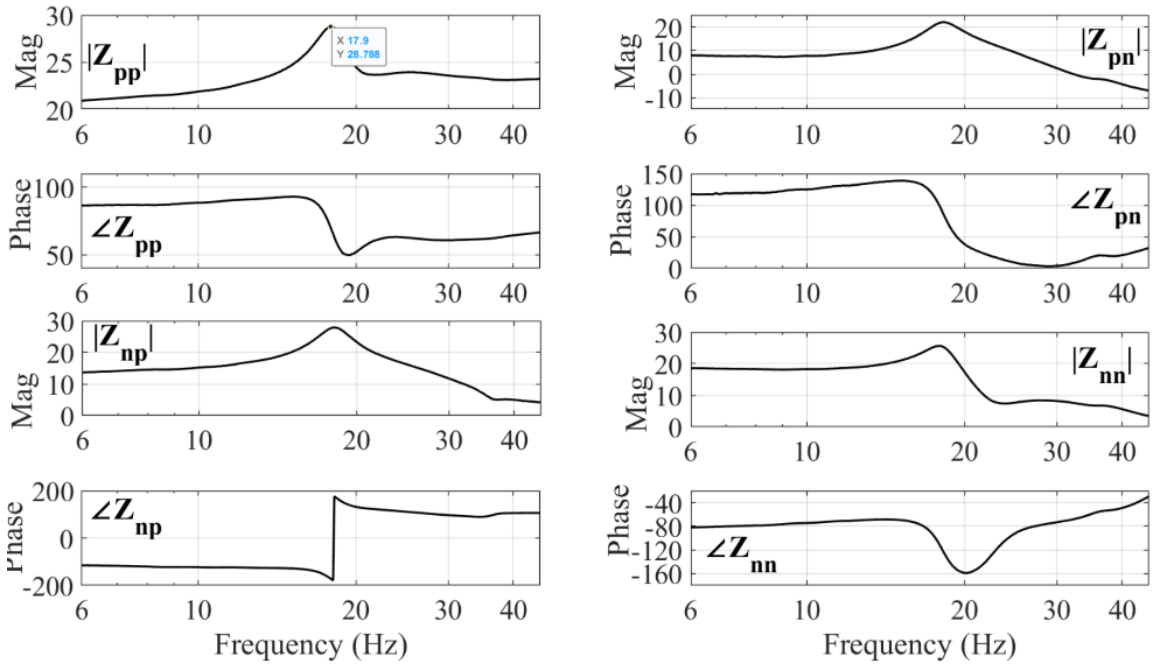

To excite the small-signal dynamics of the closed-loop system, a small variation in the grid impedance, SCR step change from 4.5 to 4, is applied at 40 s. Figure 37 shows the time domain responses of active power, reactive power, active current, and reactive current around 40 s. Figure 38 shows the FFT of the active and reactive currents from 40 to 50 s. The FFT shows a peak at 18.3 Hz at 40 s, which agrees with the 17.9 Hz magnitude peak shown in the Bode plot.

Figure 37 Stable case scenario 3, time domain simulation with SCR step change

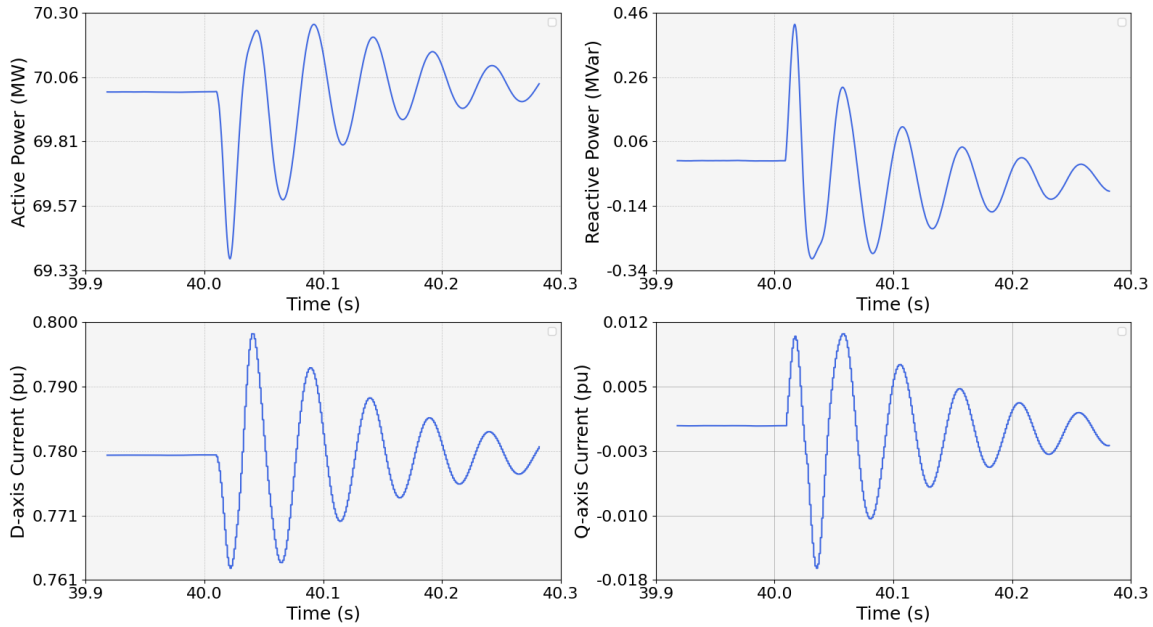

Figure 38 Stable case scenario 3, FFT of the connection point current

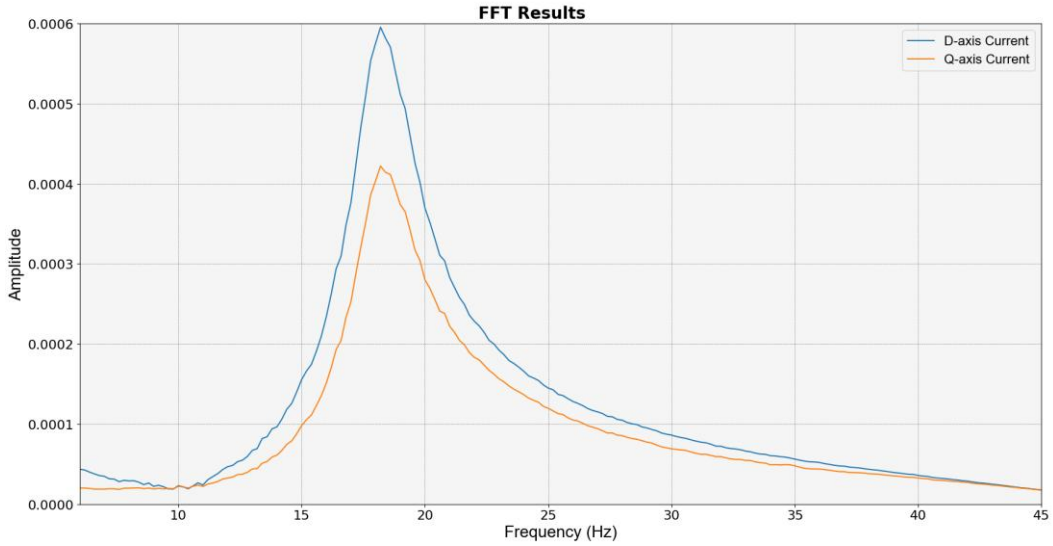

A2.1.3 Scenario 4

Figure 39 shows the GNC plot of the measured impedance ratio at PCC for scenario 4. The GNC plot is closer to the critical point (-1, j0) compared to scenario 2, indicating a decreased stability margin. Figure 40 shows the Bode plot of total impedance at the connection point. The Bode magnitude peak occurs at 17.4 Hz, indicating that the closed-loop system should have a 17.4 Hz dominant mode. Both the GNC and the Bode plot for the complete system are analysed.

Figure 39 Stable case scenario 4, GNC plot of measured impedance ratio at PCC

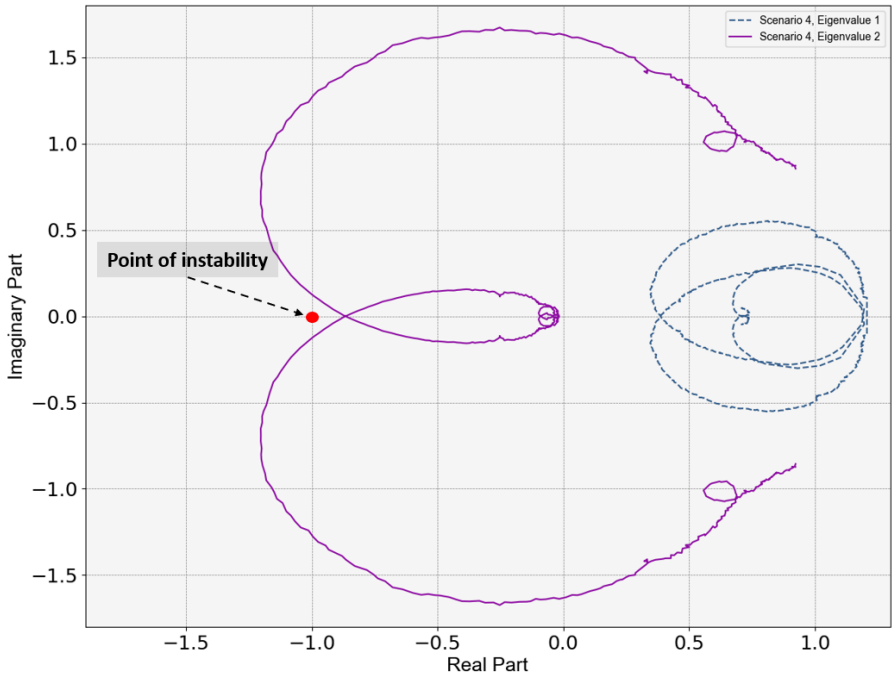

Figure 40 Stable case scenario 4, Bode plot of measured total impedance at PCC

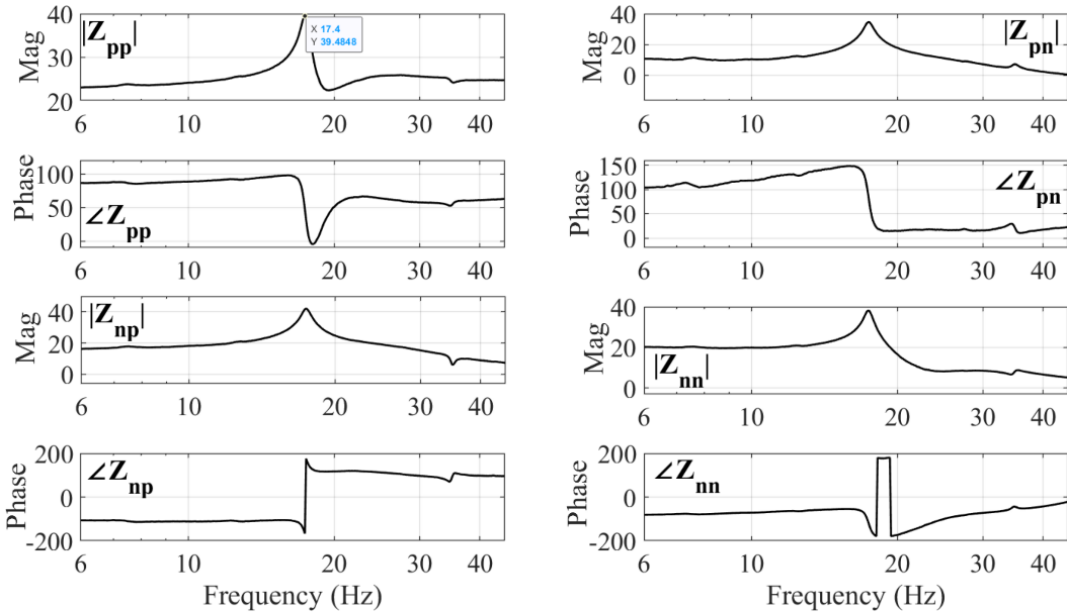

To excite the small-signal dynamics of the closed-loop system, a small variation in the grid impedance, SCR step change from 3.5 to 3, is applied at 40 s. Figure 41 shows the time domain responses of active power, reactive power, active current, and reactive current at 40 s. Figure 42 shows the FFT of the active and reactive currents from 40 to 50 s. The FFT shows a peak at 17.4 Hz at 40 s, which agrees with the 17.4 Hz magnitude peak shown in the Bode plot.

Figure 41 Stable case scenario 4, time domain simulation with SCR step change

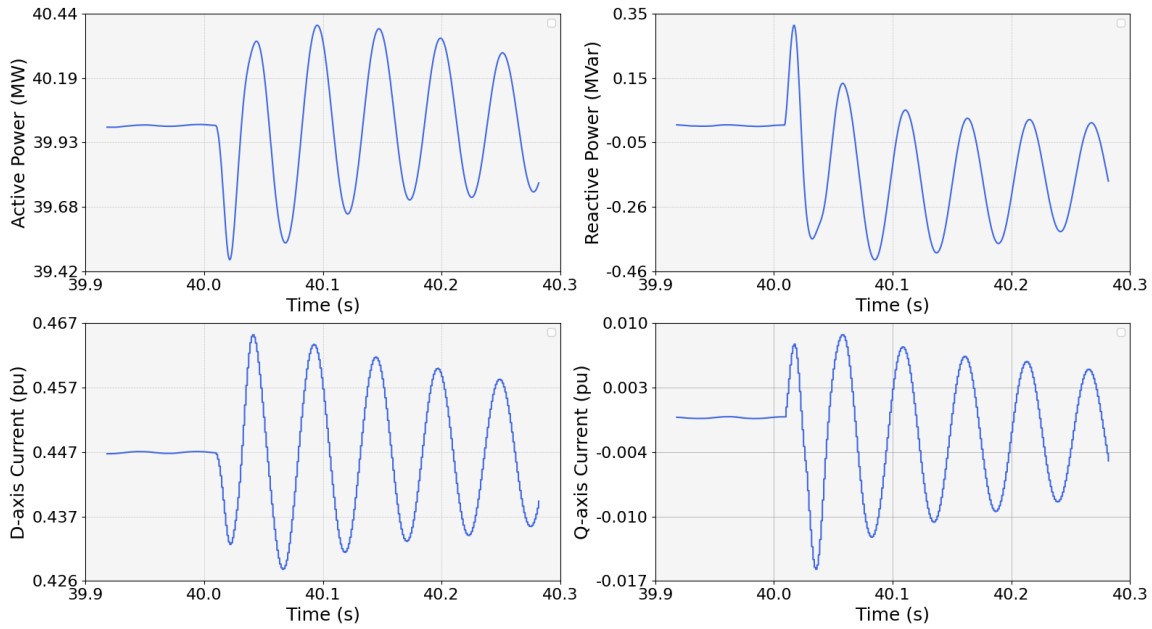

Figure 42 Stable case scenario 4, FFT of the connection point current

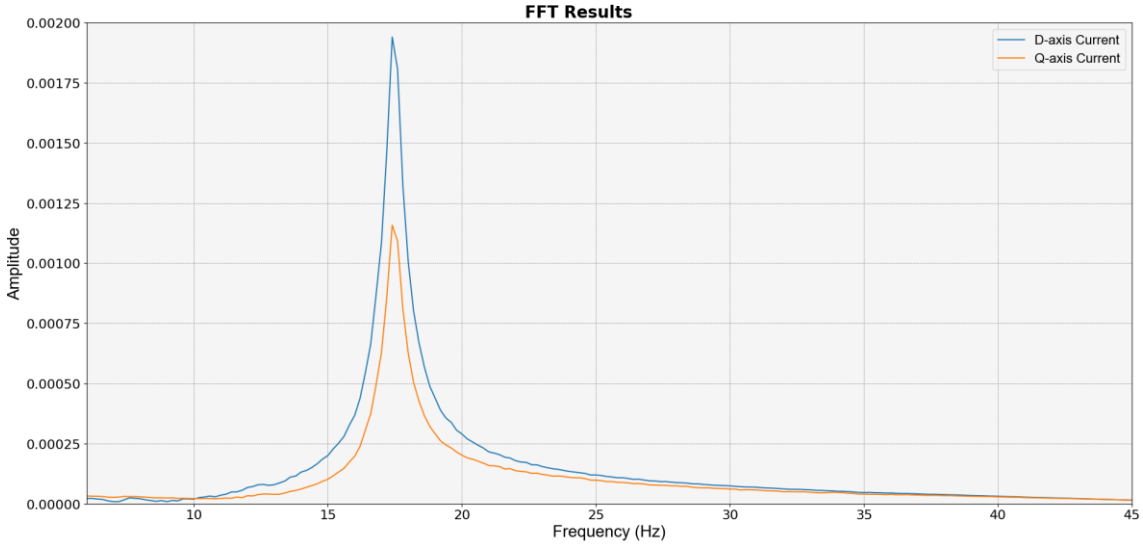

A2.2 Unstable cases validation results

A2.2.1 Scenario 2

Figure 43 shows the GNC plot of the impedance ratio at the PCC for scenario 2. The GNC plot is approaching the critical point (-1, j0) as the SCR is decreased from 3.42 to 2.55, indicating degraded stability margin as the grid impedance increases. The GNC plot encircles the critical point at a SCR of 2.51, indicating the system is unstable under this grid condition. The Bode plot in Figure 44 indicates that the system might oscillate at 17 Hz under this grid condition.

Figure 43 Unstable case scenario 2, GNC plots of impedance ratio at PCC with varied SCRs

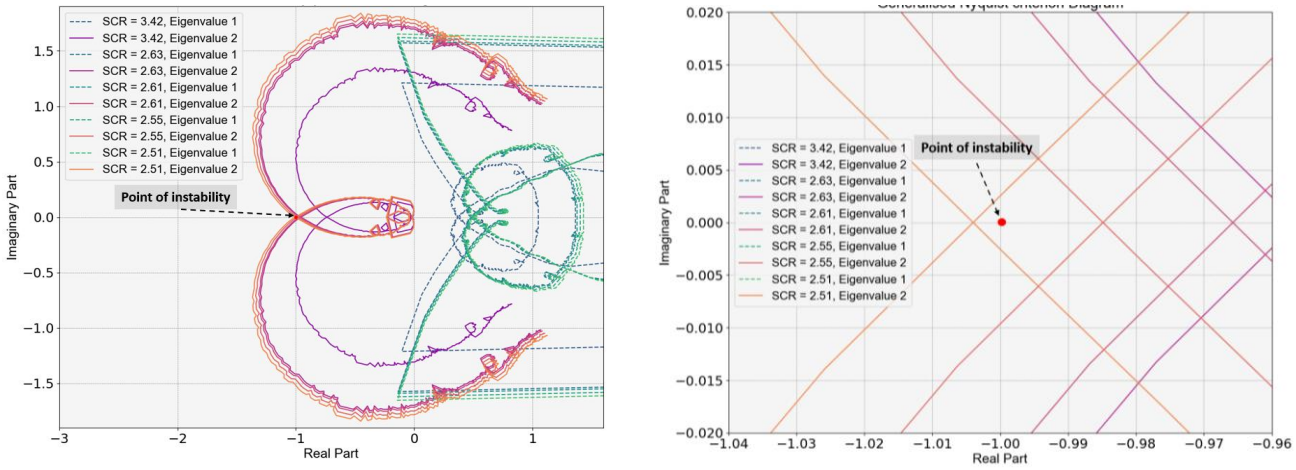

(a) Zoom out

(b) Zoom in

Figure 44 Unstable case scenario 2, Bode plots of total impedance at PCC with varied SCRs

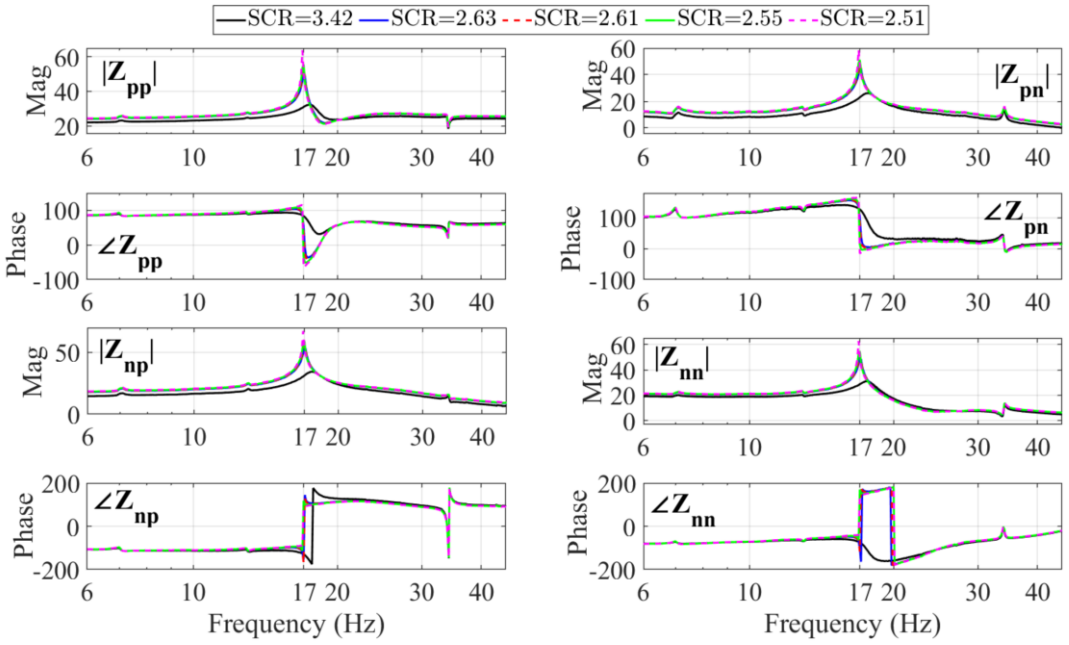

Figure 45 plots the time domain responses of active power, reactive power, active current, and reactive current under the same active and reactive power conditions as scenario 1. The irradiance is decreased from 300W/m^2 to 270 W/m^2 and the SCR is changed:

- From 3.42 to 2.61 at 40 s.
- To 2.63 at 70 s.
- To 2.55 at 100 s.
- To 2.51 at 130 s.

The stability of the system in the time domain agrees with the frequency scan analysis.

Figure 45 Unstable case scenario 2, time domain simulation results with varied SCRs

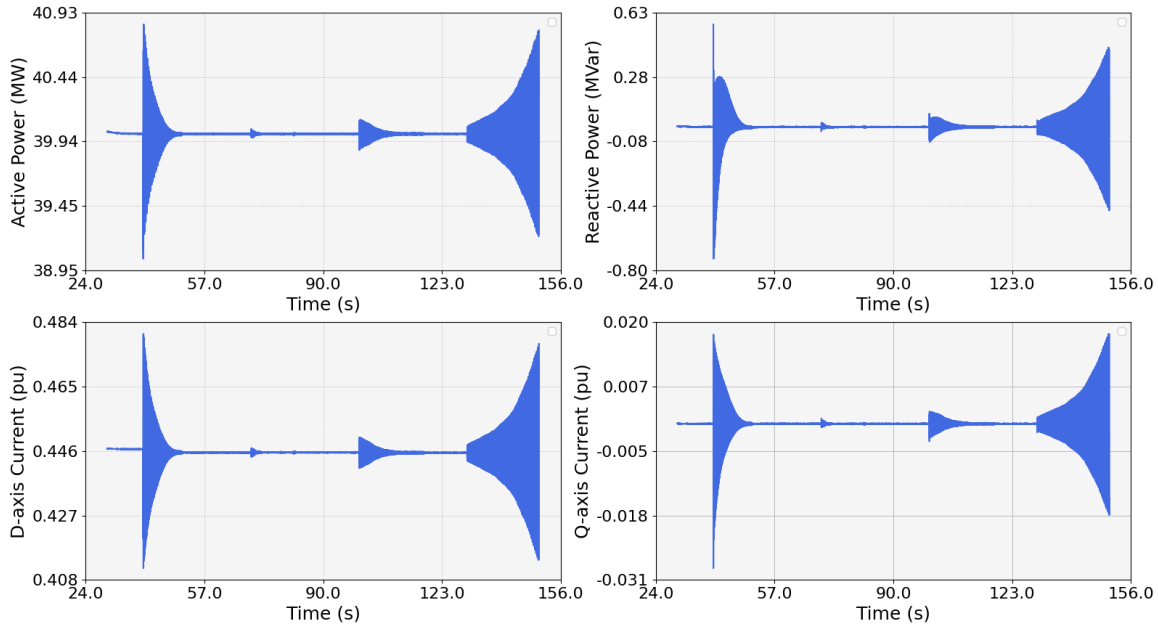

A2.2.2 Scenario 3

Figure 46 shows the GNC plot of the impedance ratio at the PCC for scenario 3. The GNC plot is approaching the critical point (-1, j0) as the SCR is decreased from 3.42 to 2.65, indicating degraded stability margin as the grid impedance increases. The GNC plot encircles the critical point at SCRs of 2.63 and 2.61, indicating the system is unstable under this grid condition. The Bode plot in Figure 47 indicates that the system might oscillate at 17 Hz under this grid condition.

Figure 46 Unstable case scenario 3, GNC plots of impedance ratio at PCC with varied SCRs

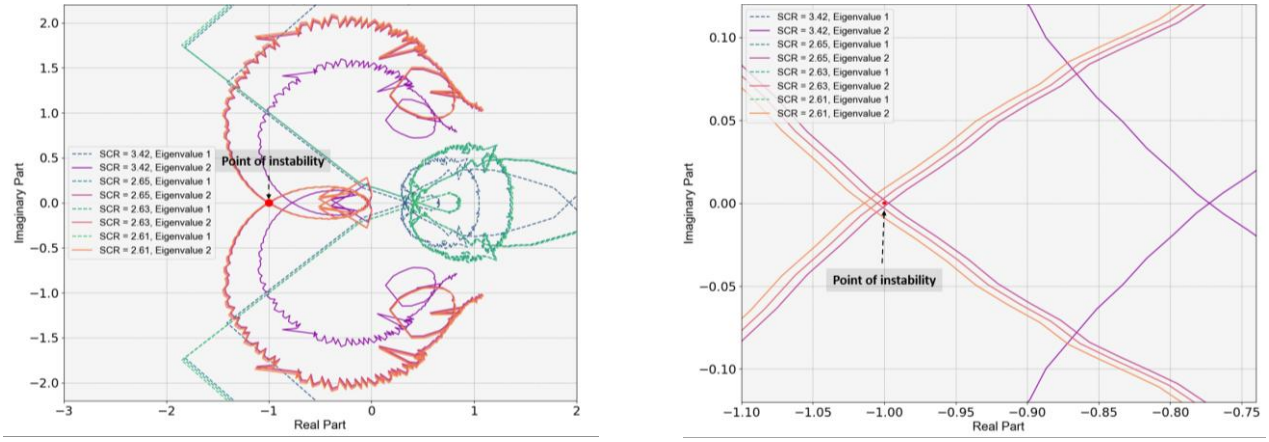

(a) Zoom out (b) Zoom in

Figure 47 Unstable case scenario 3, Bode plots of total impedance at PCC with varied SCRs

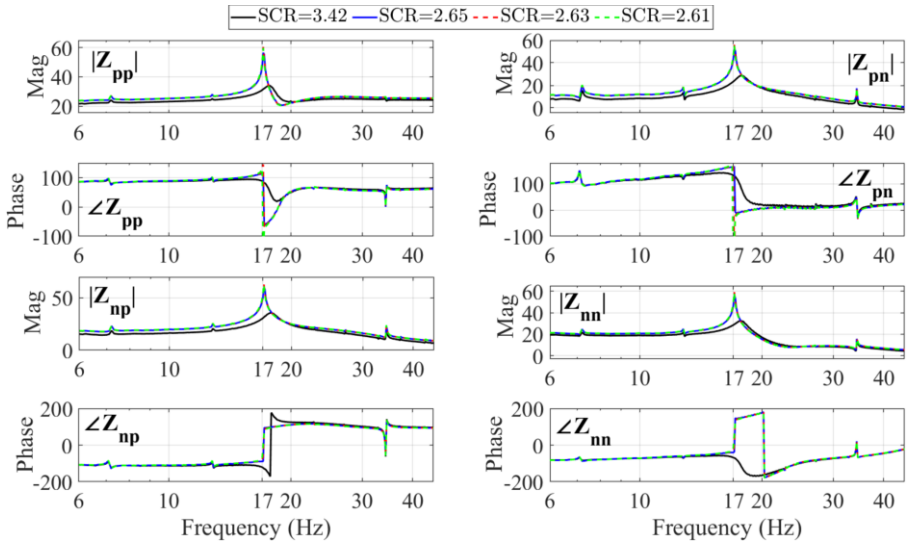

Figure 48 plots the time domain simulation results of active power, reactive power, active current, and reactive current under the same active power and reactive power conditions as scenario 1. The irradiance is increased from 300W/m^2 to 330 W/m^2 and the SCR is changed:

- From 3.42 to 2.61 at 40 s.
- To 2.63 at 70 s.
- To 2.62 at 100 s.

The stability of the system in the time domain agrees with the frequency scan analysis.

Figure 48 Unstable case scenario 3, time domain simulation results with varied SCRs

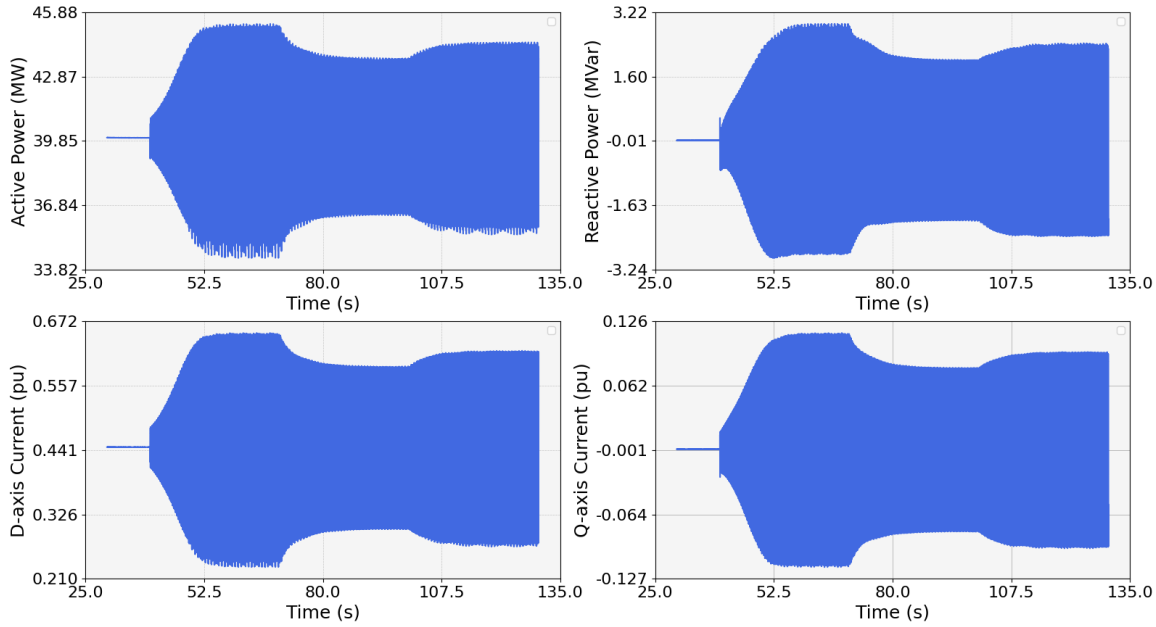

A2.2.3 Scenario 4

Figure 49 shows the GNC plot of the impedance ratio at the PCC for scenario 4. The GNC plot is approaching the critical point (-1, j0) as the SCR is decreased from 3.42 to 2.65, indicating degraded stability margin as the grid impedance increases. The GNC plot encircles the critical point as the SCR is decreased to 2.63 and 2.61, indicating that the system is unstable under both grid conditions. Furthermore, the Bode plot in Figure 50 indicates that the system might oscillate at 17 Hz under those two grid conditions.

Figure 49 Unstable case scenario 4, GNC plots of impedance ratio at PCC with varied SCRs

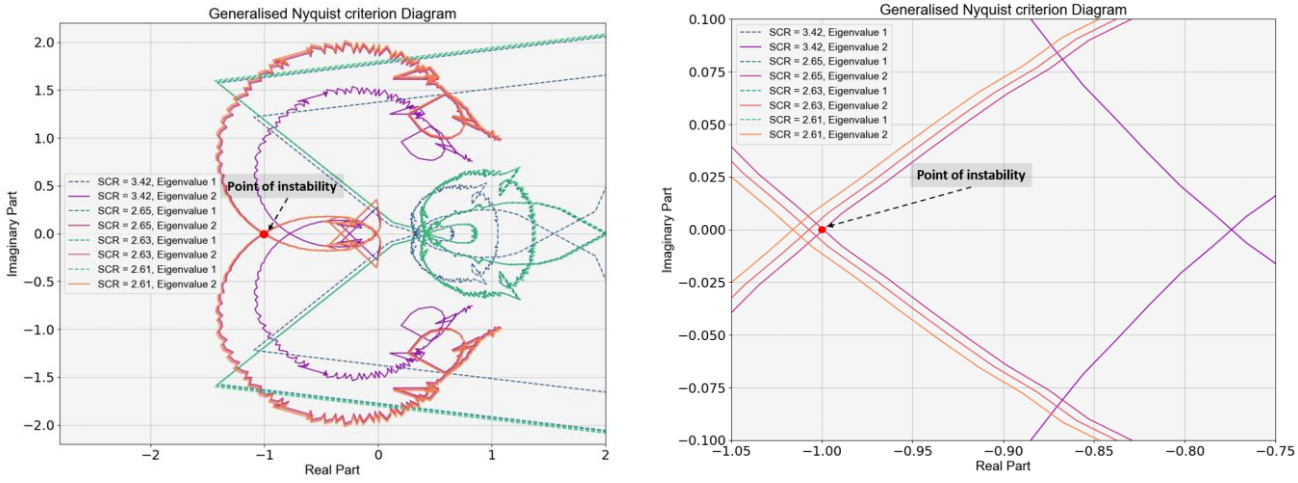

(a) Zoom out (b) Zoom in

Figure 50 Unstable case scenario 4, Bode plots of total impedance at PCC with varied SCRs

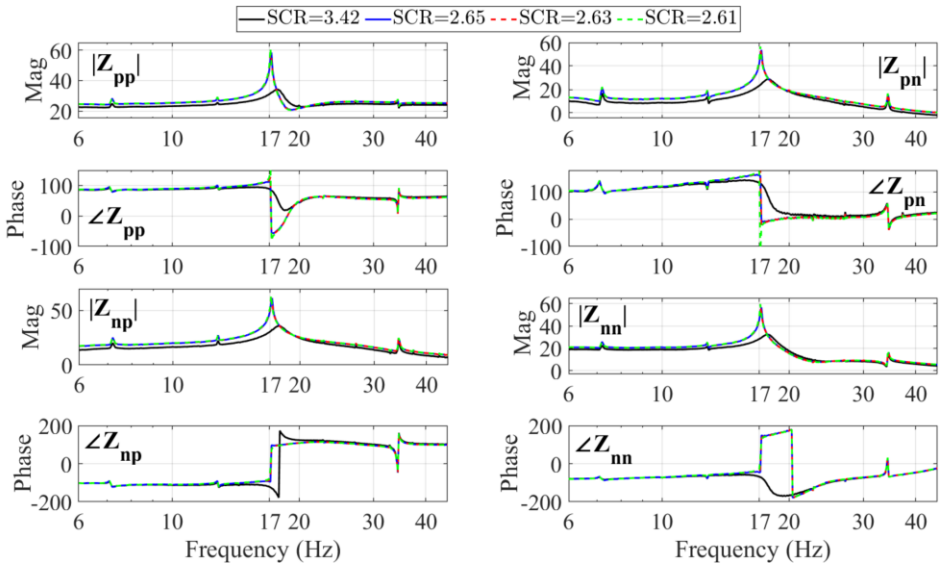

Figure 51 plots the time domain simulation results of active power, reactive power, active current, and reactive current under the same irradiance and reactive power conditions as scenario 1. The active power is decreased from 40 MW to 38 MW and the SCR is changed:

- From 3.42 to 2.61 at 40 s
- To 2.63 at 70 s.
- To 2.62 at 100 s.

The stability of the system in the time domain agrees with the frequency scan analysis.

Figure 51 Unstable case scenario 4, time domain simulation results with varied SCRs

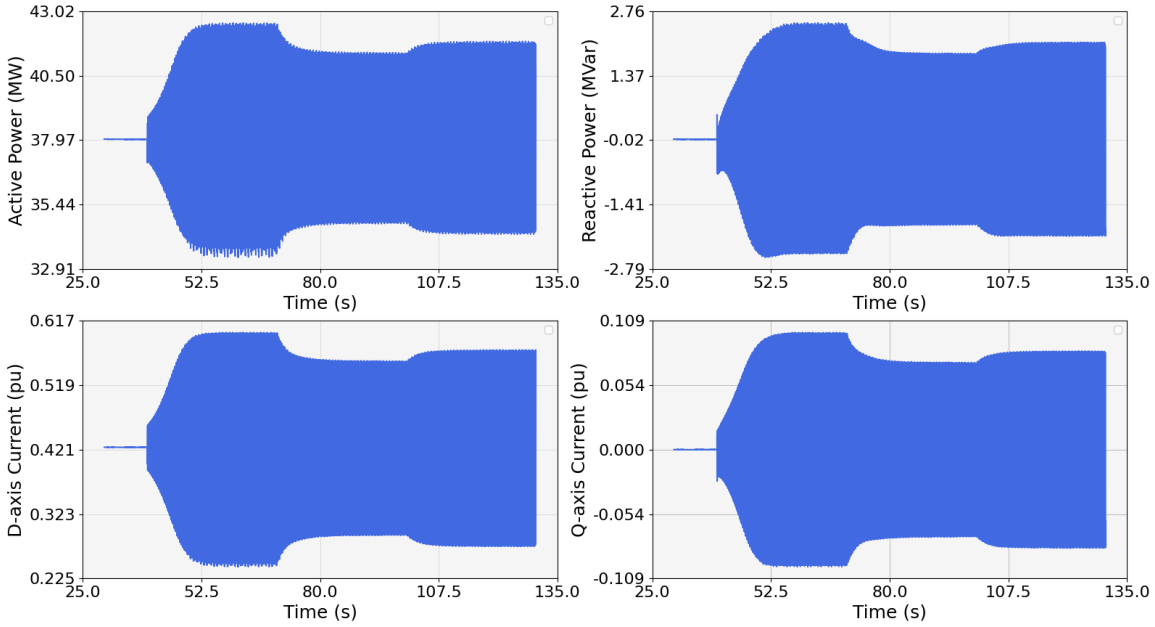

A2.2.4 Scenario 5

Figure 52 shows the GNC plot of the impedance ratio at the PCC for scenario 5. The GNC plot is approaching the critical point (-1, j0) as the SCR decreases from 3.42 to 2.55, indicating degraded stability margin as the grid impedance increases. The GNC plot encircles the critical point when the SCR is decreased to 2.51, indicating the system is unstable under this grid condition. The Bode plot in Figure 53 indicates that the system might oscillate at 17 Hz under this grid condition.

Figure 52 Unstable case scenario 5, GNC plots of impedance ratio at PCC with varied SCRs

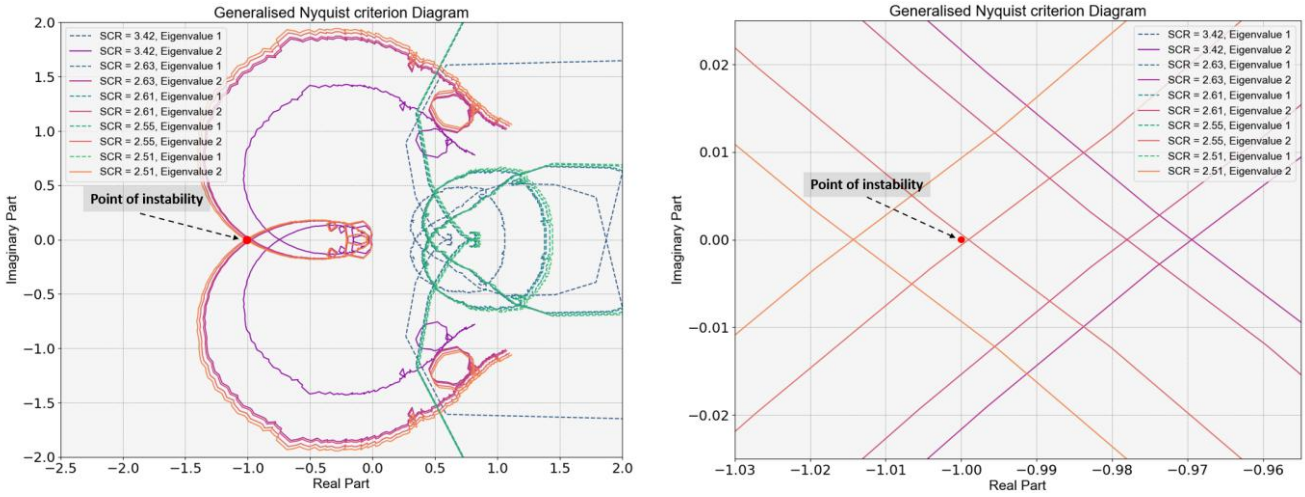

(a) Zoom out (b) Zoom-in

Figure 53 Unstable case scenario 5, Bode plots of total impedance at PCC with varied SCRs

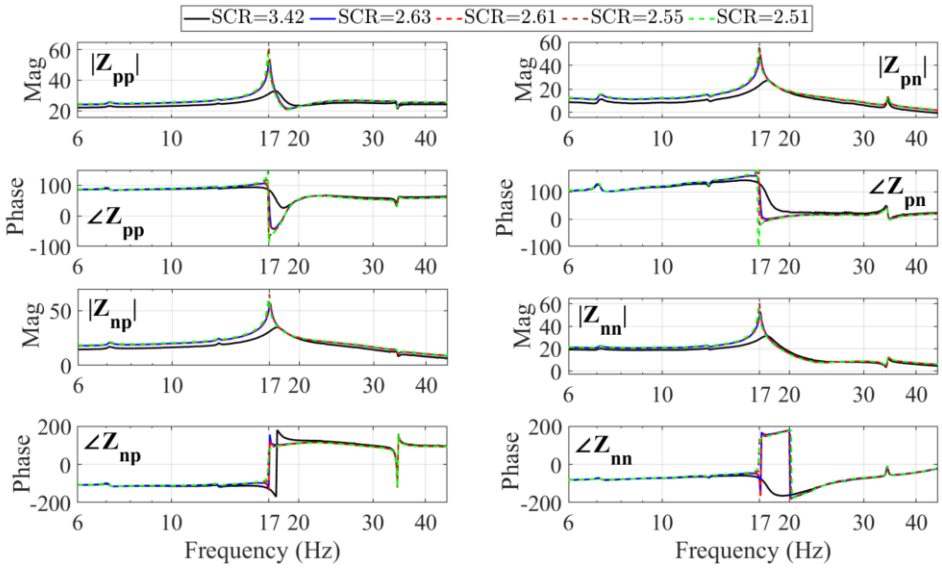

Figure 54 plots the time domain responses of active power, reactive power, active current, and reactive current under the same irradiance and reactive power conditions as scenario 1. The active power is changed from 40 MW to 42 MW and the SCR is changed:

- From 3.42 to 2.61 at 40 s
- To 2.63 at 70 s.
- To 2.55 at 100 s.
- To 2.51 at 130s.

The stability of the system in the time domain agrees with the frequency scan analysis.

Figure 54 Unstable case scenario 5, time domain simulation results with varied SCRs